TECHNICAL REPORT STANDARD TITLE PAGE

1. Report No.	2. Government Accession No.	3. Recipient's Catalog No.
CFHR 3-5-75-188-1		

4. Title and Subtitle	5. Report Date
BEHAVIOR OF STAGE-CAST INVERTED T-BEAMS WITH THE PRECAST FLANGE IN TENSION	August 1976
	6. Performing Organization Code
7. Author(s)	8. Performing Organization Report No.
S. A. A. Wahidi and R. W. Furlong	Research Report 188-1
9. Performing Organization Name and Address	10. Work Unit No.
Center for Highway Research The University of Texas at Austin Austin, Texas 78712	11. Contract or Grant No. Research Study 3-5-75-188
	13. Type of Report and Period Covered
12. Sponsoring Agency Name and Address	Interim
Texas State Department of Highways and Public Transportation; Transportation Planning Division P. O. Box 5051 Austin, Texas 78763	14. Sponsoring Agency Code

15. Supplementary Notes

Work done in cooperation with the Department of Transportation, Federal Highway Administration. Research Study Title: "Failure Criteria for Precast Elements of Composite Inverted T-Beams"

16. Abstract

The test program was intended to demonstrate the flexural behavior of stage-cast inverted T-beams constructed with a web cast in place against a preloaded flange. Four reinforced concrete T-beams were subjected to loads that caused compression in the web and tension in the flanges. Two of the specimens were stage-cast, while the other two, called control specimens, were monolithically cast and had the same size and reinforcement as the stage-cast beams. The behavior of stage-cast specimens was compared with that of similar control specimens to observe differences of ultimate strength, ductility, stiffness under live loads, and the extent and size of cracks.

17. Key Words	18. Distribution Statement
inverted T-beams, stage-cast, precast flange, tension, flexural loading, web	No restrictions. This document is available to the public through the National Technical Information Service, Springfield, Virginia 22161.

19. Security Classif. (of this report)	20. Security Classif. (of this page)	21. No. of Pages	22. Price
Unclassified	Unclassified	106	

Form DOT F 1700.7 (8-69)

BEHAVIOR OF STAGE-CAST INVERTED T-BEAMS WITH THE PRECAST FLANGE IN TENSION

by

S. A. A. Wahidi and R. W. Furlong

Research Report 188-1

Project 3-5-75-188
Failure Criteria for Precast Elements of Composite Inverted T-Beams

Conducted for

Texas
State Department of Highways and Public Transportation

In Cooperation with the
U. S. Department of Transportation
Federal Highway Administration

by

CENTER FOR HIGHWAY RESEARCH
THE UNIVERSITY OF TEXAS AT AUSTIN

August 1976

The contents of this report reflect the views of the authors, who are responsible for the facts and the accuracy of the data presented herein. The contents do not necessarily reflect the official views or policies of the Federal Highway Administration. This report does not constitute a standard, specification, or regulation.

S U M M A R Y

This Interim Report contains a description of physical tests, data interpretation, and conclusions regarding stage cast inverted T-beams subjected to positive moment flexural loading that created tension in the flange of the T-beams. The Final Report of the project will include similar information for inverted T-beams subjected to negative moment flexural loading that created compression in the flange of the T-beams.

The behavior of two inverted T-beam bent cap models that were constructed in two stages was compared with identical models that had been monolithically cast in one stage. The first stage involved construction and loading of a flange and the second stage involved construction of the web on the loaded flange. The models had identical web dimensions but the flanges of one pair were almost twice as thick as the flanges of the other pair.

IMPLEMENTATION

For the size and reinforcement ratios of the specimens tested, significant conclusions regarding positive moment behavior included:

(1) The maximum crack size in stage cast beams at service live load was greater than the crack size of monolithically cast beams.

(2) The stage cast beams displayed a greater number of cracks than monolithically cast beams, but very few cracks from preloaded flanges penetrated into webs of stage cast members.

(3) The live load stiffness of stage cast beams was roughly double that of monolithically cast beams.

(4) Stage cast beams yielded in flexure at a live load 30 percent lower than that required to yield monolithically cast beams.

(5) The effects of preloading must be considered for estimating the yield strength of stage cast beams.

(6) Stage cast beams exhibited 50 to 70 percent more ductility than monolithically cast beams.

(7) The ultimate flexural strength of inverted T-beams is not influenced by stage casting. The effects of preloading could have been neglected in the analysis of capacity. Concrete rectangular stress block theory could be applied reasonably for all four beams.

These conclusions apply for positive moment flexural behavior of specimens for which nominal dead loads from stringers were 15 to 30 percent of total design loads. Bridges with higher ratios of dead load to total load on bent caps should include a separate "construction load" analysis for the safety of stage-cast inverted T-beam flanges under positive moment.

A B S T R A C T

The test program was intended to demonstrate the flexural behavior of stage-cast inverted T-beams constructed with a web cast in place against a preloaded flange. Four reinforced concrete T-beams were subjected to loads that caused compression in the web and tension in the flanges. Two of the specimens were stage-cast, while the other two, called control specimens, were monolithically cast and had the same size and reinforcement as the stage-cast beams. The behavior of stage-cast specimens was compared with that of similar control specimens to observe differences of ultimate strength, ductility, stiffness under live loads, and the extent and size of cracks.

For the size and steel ratio of the specimens tested, the following conclusions were made:

(1) The variation of strain along the depth of a beam subjected to positive moments was found to be close to a straight line.

(2) The maximum crack size in stage-cast beams at low live loads was more than that in the monolithic beams.

Maximum crack width in stage-cast beams at service loads was less than that permitted by CEB (European Committee on Concrete) for ordinary conditions. In very aggressive atmospheric conditions, however, stage-cast beams with span to overall thickness ratio greater than 16 may have corrosion problems.

(3) The typical crack spacing was the same for the stage-cast and control specimens in the case of beams with an 11-in. thick flange. Cracks occurred closer together in the stage-cast specimens than in the control specimens for beams with 6-in. thick flanges.

The total number of cracks in the flange was larger in the case of stage-cast beams, but very few of the cracks in stage-cast beams extended into the web even at high loads.

(4) Stage-cast specimens subjected to changes in service live loads appeared to be twice as stiff as the control specimens.

(5) The ultimate moment of stage-cast specimens was approximately equal to that of the control specimens. However, yielding of steel in stage-cast specimens took place at a load up to 30 percent less than that required to yield the tension steel of the control specimens.

(6) Stage-cast specimens exhibited 1.5 to 1.7 times as much ductility as their monolithically cast counterparts did before failure.

(7) Effects of preloading can be neglected in the design of stage-cast beams, and the same design procedure as that used for monolithic beams can be used to design stage-cast beams. The use of a rectangular stress block to represent concrete stress at ultimate seems to be reasonable.

(8) For estimating the yield load of stage-cast beams, the effects of the preloading of flange must be taken into account. Elastic theory may be used for analysis of stage-cast beams at loads less than loads that cause tension steel to yield.

C O N T E N T S

LIST OF TABLES

LIST OF FIGURES

N O T A T I O N S

A	Area, $in.^2$
A_g	Gross area of section, $in.^2$
A_s	Area of tension reinforcement, $in.^2$
A'_s	Area of compression reinforcement, $in.^2$
A_{sf}	Area of tension reinforcement for flange section, $in.^2$
A'_{sf}	Area of compression reinforcement in flange, $in.^2$
A'_{sw}	Area of compression reinforcement in web, $in.^2$
A_v	Area of shear reinforcement within a distance s, $in.^2$
A_{vf}	Area of shear-friction reinforcement, $in.^2$
a	Depth of equivalent rectangular stress block, in.
a_f	Distance of line of action of flange load from the face of web, in.
b	Width of compression face of member, in.
b_f	Width of flange, in.
b_v	Width of the cross section being investigated for horizontal shear, in.
b_w	Web width, in.
C	Total internal compression force at a section, kips
C_c	Internal compression force resisted by the concrete, kips
C_{cf}	Internal compression force in flange resisted by the concrete, kips
C_{cw}	Internal compression force in web resisted by concrete, kips
C_s	Internal compression force resisted by steel, kips
C_{sf}	Internal compression force in flange resisted by steel, kips
C_{sw}	Internal compression force in web resisted by steel, kips
c	Distance from extreme compression fiber to neutral axis, in.
c_f	Distance from extreme compression fiber of flange to the neutral axis in the flange, in.
c_w	Distance from extreme compression fiber of web to the neutral axis in web, in.
d	Distance from extreme compression fiber to the centroid of tension reinforcement, in.

d'	Distance from extreme compression fiber to centroid of compression reinforcement, in.
d_f	Distance from extreme compression fiber of flange to centroid of tension reinforcement in flange, in.
d'_f	Distance from extreme compression fiber of flange to centroid of compression reinforcement in flange, in.
d_w	Overall depth of web, in.
E_c	Modulus of elasticity of concrete, ksi
E_{cf}	Modulus of elasticity of concrete in flange of stage-cast beam, ksi
E_{cw}	Modulus of elasticity of concrete in web of stage-cast beam, ksi
E_s	Mosulus of elasticity of steel, ksi
F	$(d + b_w)A_v f_y/s$, kips
f	Stress, ksi
f_{av}	Average bending stress in flange, ksi
f_c	Compressive stress in concrete, psi or ksi
f'_c	Crushing strength of concrete cylinders, psi
f''_c	Maximum stress in flexure, psi
f_{cf}	Compressive stress in concrete at the extreme compression fiber of flange, psi
f'_{cf}	Crushing strength of cylinders for concrete used in the flange of stage-cast beam, psi
f_{cw}	Compressive stress in concrete at the extreme compression fiber of web, psi
f'_{cw}	Crushing strength of cylinders for the concrete used in the web of stage-cast beam, psi
f_r	Modulus of rupture of concrete, psi
f_s	Calculated tensile stress in steel, ksi
f'_s	Calculated compressive stress in steel, ksi
f_y	Yield strength of reinforcement, ksi
h	Overall depth of the T-section, in.
I	Moment of inertia of section, $in.^4$
jd	Lever arm, in.
jd_f	Lever arm for the internal couple in flange, in.
M	Moment, kip-in.

M_f	Moment in projected portion of flange due to bracket load P_b, kip-in.
M_u	Applied ultimate moment, kip-in.
M'_u	Ultimate moment capacity of the section, kip-in.
M_y	Applied moment at which tension steel yields, kip-in.
n	Modular ratio, E_s/E_c
P	Applied load, kips
P_D	Design dead load at each load point = $P_f/4$, kips
P_L	Design live load at each load point = $P_w/2$, kips
P_f	Maximum total applied load on flange, kips
P_u	Total ultimate load, kips
P_w	Total applied web load at ultimate, kips
p	Ratio of tension reinforcement = A_s/bd
p'	Ratio of compression reinforcement = A'_s/bd
p_b	Reinforcement ratio producing balanced conditions
p_f	Reinforcement ratio for flange section = $A_{sf}/b_f d_f$
p_w	Reinforcement ratio for nonrectangular sections = $A_s/b_w d$
s	Center-to-center spacing of stirrups, in.
T	Total internal tension force, kips
t_f	Overall thickness of flange, in.
V	Shear force, kips
V_f	$2\sqrt{f'_c}\, b_f d_f + A_v d_f f_y/s$, kips
V_h	Design horizontal shear force, kips
V_u	Total applied design shear force, kips
v	Shear stress, ksi
v_c	Nominal permissible shear stress carried by concrete, ksi
v_{dh}	Design horizontal shear stress at any cross section, ksi
v_h	Permissible horizontal shear stress, ksi
v_s	Design shear stress to be carried by the shear reinforcement, ksi
v_u	Nominal total design shear stress, ksi
w	Dimension of flange loading plate in a direction parallel to the span, in.
$\bar{x}$	Distance from neutral axis to centroid of the compression force carried by concrete, in.

$\bar{x}_f$	Distance from flange neutral axis to centroid of compression force carried by concrete in flange, in.
$\bar{x}_w$	Distance from web neutral axis to centroid of compression force carried by concrete in web, in.
y	Distance of any point from neutral axis, in.
Δ	Deflection at midspan, in.
ϵ	Strain, in./in.
ϵ_c	Strain in concrete, in./in.
ϵ_{cf}	Resultant strain in concrete at web-flange interface, in./in.
ϵ_{ci}	Initial compressive strain in concrete at the top fiber of flange caused by the preload, in./in.
ϵ_{cu}	Maximum compressive strain in concrete at ultimate load, in./in.
ϵ_{IF}	Change in strain at web-flange interface, caused by web loads, in./in.
ϵ_o	Strain in concrete corresponding to a concrete stress equal to f''_c, in./in.
ϵ_{of}	ϵ_o for the concrete used in flange of stage-cast beam, in./in.
ϵ_{ow}	ϵ_o for concrete used in web of stage-cast beam, in./in.
ϵ_s	Strain in tension reinforcement, in./in.
ϵ'_s	Strain in compression reinforcement, in./in.
ϵ'_{sf}	Resultant strain in steel placed near the top of flange, in./in.
ϵ_{si}	Initial strain in tension reinforcement, in./in.
ϵ_{sw}	Change in strain in tension reinforcement caused by the application of web loads, in./in.
ϵ'_{sw}	Strain in compression steel in web, in./in.
ϵ_y	Strain in reinforcement at yielding, in./in.
μ	Coefficient of friction
φ	Curvature at midspan, rad/in.
$\bar{\varphi}$	Strength reduction factor
φ_f	Curvature of flange of stage-cast beam at midspan, rad/in.
φ_w	Change in midspan curvature caused by web loads, rad/in.

CHAPTER 1

INTRODUCTION

1.1 General

The purpose of this report is to study the flexural behavior of stage-cast reinforced concrete inverted T-beams. A stage-cast T-beam is a reinforced concrete T-beam constructed with a web cast in place against a preloaded flange. Stage-cast inverted T-beams are commonly used as structural members, such as bent cap girders in highway bridges to support prestressed concrete stringers, as shown in Fig. 1.1. The bridge construction procedure involves an inverted T-beam bent cap constructed by using the flange as a structural member to support stringers and formwork for the cast-in-place web of the stage-cast T-beam. By casting the bent cap web with the stringers, the cost of separate diaphragms for each stringer can be saved.

In the cantilevered portion of a bent cap the bottom portion of the flange is put into compression as it supports the stringers, formwork, its own weight, and the weight of the deck slab and web before the web gains strength. Although these stresses (and strains) may be quite high in magnitude because of the comparatively small depth of the flange, they are never relieved before traffic loads are permitted to create still more compression in the flange which now acts compositely with the web. The flange portion which was in tension during construction may provide some compression reserve, but only if the neutral axis of the composite section at ultimate load is farther from the compression face than the neutral axis of the flange during the first stage (construction) loading.

In positive moment regions the bottom steel is required to resist the stresses due to construction loads prior to hardening of

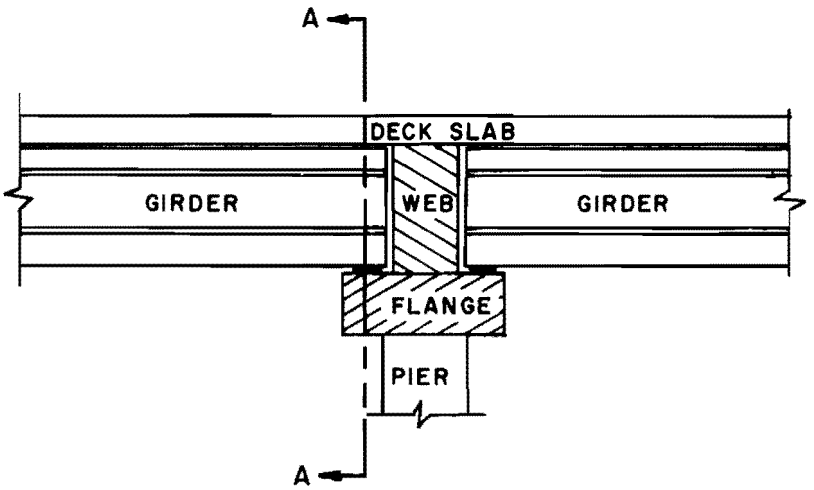

(a) SIDE VIEW

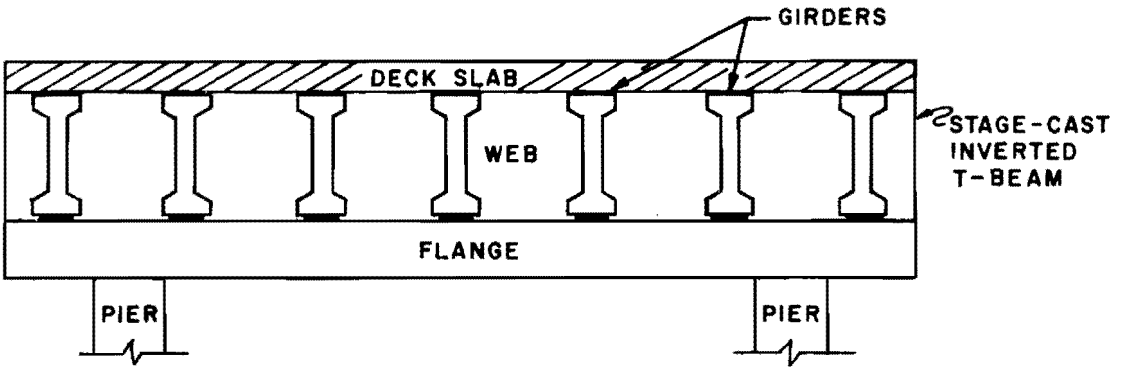

(b) SECTION A-A

Fig. 1.1 Highway bridge bent cap

the web. As the lever arm of the flange section is much smaller than that of the T-section, the high tensile strain in the steel will permit flexural cracks in the flange. These cracks are never relieved before the traffic loads are permitted to cause additional tension in the same steel when it acts as the reinforcement for the T-section. Since crack width is related more to steel strain and concrete cover than to strain gradient, it is possible that live loads on the stage-cast T-section may extend and widen the already large dead load cracks to unacceptable sizes. However, the precompressed zone of concrete in the flange may help in restraining the further extension of dead load cracks when the precompressed upper portion of the flange becomes a part of the tension zone of the composite T-section. The extent and size of web cracks in a stage-cast inverted T-beam may also be affected by the thickness of the flange. The precompressed zone of a thicker flange would be closer to the neutral axis of the composite T-section and may restrain the size and extent of web cracks more effectively. Due to the nonplanar strain distribution and crack propagation, a stage-cast beam might have a different stiffness under live loads than that of a monolithically cast one. The stiffness for live load may also be dependent on the flange thickness-to-depth (of T-section) ratio. Deflections, crack width, and cracking extent may depend also upon the creep effect created by construction loads on a comparatively shallow and highly stressed flange. Any creep effect will be more prominent for comparatively thin flanges. Furthermore, high stresses in tension steel produced by the preloading of a flange during construction may cause the steel of stage-cast beams to yield at a lower live load than for a similar monolithic beam. This would, however, ensure a greater ductility, since the ultimate load is expected to be approximately equal for similar stage-cast and monolithic beams. The reduction of yield load and increment of ductility are expected to be larger for beams having greater ratios of flange thickness-to-depth of T-section.

This report attempts to investigate the behavior of stage-cast inverted T-beams subjected to positive moments only, by comparing the

behavior of stage-cast beams with that of similar monolithically cast ones. Beams of two different flange thicknesses were tested in order to study the effect of strain gradient on crack development, crack size, stiffness for live load, ductility, and strength of the composite T-section. Specimens of different flange thicknesses should also furnish information regarding creep in the flange during construction loading and its effect on the serviceability of the composite, stage-cast beam.

1.2 Previous Studies on Composite Flexural Members

The behavior of composite or stage-cast concrete flexural members has been studied extensively in the past.[6,7,8,9,10,11,12] Most of the studies presented so far deal with shear transfer between precast and cast-in-place components,[7,9,12] and almost all of the research involves a cast-in-place slab and a precast web.[6, 7,8,10,11,12] The present study is directed towards the behavior of a beam with a cast-in-place web and a preloaded (precast) flange. A preloaded flange has a high level of stresses and strains, as well as considerable cracking prior to the casting of the web. This is entirely different from the case of a slab cast over a precast, preloaded web and has not been studied so far. A cast-in-place web and precast flange also involve a considerable change in the effective depth and effective internal moment lever arm of the composite member.

1.3 Objectives of the Study

The objectives of the test program were as follows:

(1) To investigate whether the size of cracks in stage-cast beams is acceptably small after composite tensile strains are superimposed on to "locked-in" tensile strains at the bottom of the flange.

(2) To investigate the effect of the ratio between flange thickness (relative depth of precompressed zone) to total depth of T-section, on size and propagation of cracks.

(3) To compare the stiffness of cracked stage-cast T-beams with that of similar monolithic beams subjected to live loads, and to study the effect of relative flange thickness on the stiffness of stage-cast beams.

(4) To compare the ductility of stage-cast beams to that of monolithic beams and to find out if ductility of stage-cast beams depends upon the flange thickness.

(5) To determine whether the traditional rectangular stress block and a strain limit of 0.003 are reliable analytical tools for evaluating the ultimate strength of stage-cast members subjected to positive moments.

(6) To investigate whether a simple design procedure which ignores the initial strains in a preloaded flange is adequate to design simply supported stage-cast inverted T-beams. Will such beams have sufficient strength, stiffness, and ductility? If so, will such beams have crack widths small enough to be acceptable?

CHAPTER 2

SPECIMEN DETAILS AND TEST SETUP

2.1 General

The tests were carried out at the Civil Engineering Structures Research Laboratory of The University of Texas at Austin. Four beams were tested. Two had a flange thickness of 6 in. and an overall depth of 22 in., and two had flanges 11 in. thick with an overall depth of 27 in. One beam of each size was cast in two stages--the flange was cast, cured, and loaded until tensile steel reached a 45 ksi tension stress, prior to the casting of the web. The loads on the flange were maintained during casting and curing of the web. A companion specimen for each stage-cast beam was cast in only one stage--the web and flange were cast monolithically at the same time. These beams, referred to in this report as control specimens, were used to compare the behavior of the corresponding stage-cast beams (or specimens). The control specimens were reinforced exactly like their respective stage-cast counterparts; also, maximum care was taken to ensure that concrete mix of approximately the same strength was used for beams of the same size. The beams were designated as BMS1, BMS2, BMSP1, and BMSP2, where BM stands for "beam," S for support condition--"simply supported," the letter P (if present) indicates that the web of the beam was cast against the precast, preloaded flange (i.e., the beam was cast in two stages), and numbers 1 and 2 indicate the flange thickness; 1 indicates a 6 in. thick flange, and 2 indicates an 11 in. thick flange.

2.2 Test Specimens

2.2.1 Size. Specimens of two different flange thicknesses were used to investigate the effect of flange thickness on crack size, crack propagation, creep due to construction load, stiffness for live

load, ductility and strength of stage-cast beams. Flange thicknesses of 6 in. and 11 in. were chosen in order to make the effective depth of 11 in. flange section (d = 9.625 in.) approximately twice that of the 6 in. flange (d = 4.75 in.). A 16-in. deep web was selected for all the specimens to make the dimensions of the beam proportional to those usually adopted for high bridge bent caps.

All specimens had a span of 110 in. and were loaded at two sections, 40 in. from either support.

2.2.2 Design Criteria. Main Reinforcement. A load equivalent to 45 ksi stress in the tension steel was to be sustained on the flanges of stage-cast beams before the casting of the web; the steel ratio (computed by using breadth and depth of the flange section) equal to 60 percent of that required to produce a balanced (flange) section was, therefore, adopted for the tension reinforcement to provide an adequate compression reserve for the section under sustained loads. This steel ratio was found to be equal to 0.0171 for f'_c of 4000 psi and f_y of 60000 psi. Nine #4 bars for 6 in. flange and nine #6 bars for 11. in. flange sections were selected, accordingly. The same reinforcement was adopted for the control specimens. The section was then analyzed to compute the magnitude of the load which would produce a stress of 45 ksi in the tension steel--45 ksi was considered to be an upper limit to the stress in Grade 60 steel at service dead loads for the load factor of 1.30 suggested by AASHTO specifications. The stress in concrete was checked at this load and was found to be 3200 psi (0.8 times f'_c) for a 6 in. flange and 3340 psi (0.835 times f'_c) for an 11 in. flange section. Appendix A-1 shows the design calculations for beams BMS1 and BMSP1. Similar calculations were made for BMS2 and BMSP2.

Ductility of the beams was investigated at ultimate load (using properties of the T-section). The steel ratio for the T-sections was found to be less than $0.75p_b$, as suggested by ACI 318-71, which assured yielding of steel before crushing of concrete. The T-section was analyzed to predict the load at yielding of steel and that at

compression failure. Figures 2.1 and 2.2 show the dimensions, reinforcement, and the load predicted to fail the beams in compression.

Shear and Bracket Reinforcement. Shear and bracket reinforcements were designed to carry 25 percent more load than that predicted for the flexural failure. This was done in order to ensure a flexural failure of the specimens. The web reinforcement was designed for vertical shear, shear transfer between web and flange, horizontal shear at web-flange interface and for supporting the flange load by hanger action. Separate shear reinforcement was provided in the flange to resist the shears due to flange loads. Horizontal bars normal to the axis of the beam were designed to provide flexure and shear reinforcement for bracket action of the projected portion of the flange. The design of all reinforcement was based on f_y of 60 ksi.

Design computations are shown in Appendix A-1 and details of reinforcement are shown in Figs. 2.1 and 2.2.

2.2.3 Actual Dimensions and Reinforcement. The desired dimensions of the specimen were as shown in Figs. 2.1 and 2.2. Due to imperfections of the forms, the actual dimensions of the specimens differed slightly from the desired ones. Also, the webs of the stage-cast specimens were deeper at midspan than at the ends, due to the adopted method of construction, explained in detail in Sec. 2.2.4, Table 2.1(a) shows the actual dimensions of the specimens.

Specimens BMS1 and BMSP1 (flange thickness = 6 in.) contained nine #4 Grade 60 longitudinal bars as tension reinforcement (area = 1.77 sq. in.). Two #4 bars were placed near the top of the web and two #4's near the top of the flange in order to support the shear reinforcement at the time of casting. The web reinforcement consisted of twenty-four #3 closed stirrups (2 legs) at 5 in. center-to-center. Twelve #3 U-shaped bars at 10 in. center-to-center were provided to act as the shear reinforcement for the preloaded flange, prior to the casting of the web. Twelve #3 straight bars at 10 in. center-to-center

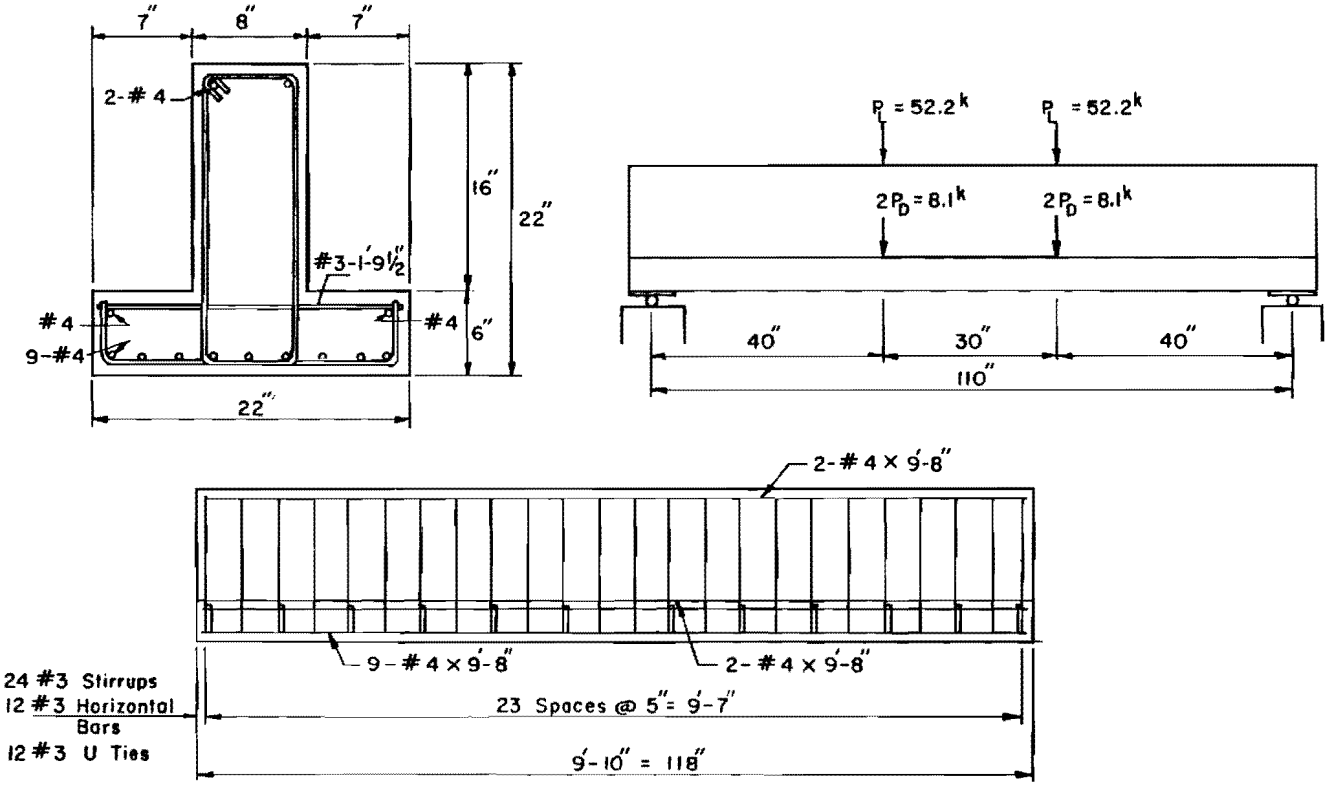

Fig. 2.1 Dimensions, reinforcement, and predicted maximum loads for Beams BMS1 and BMSP1

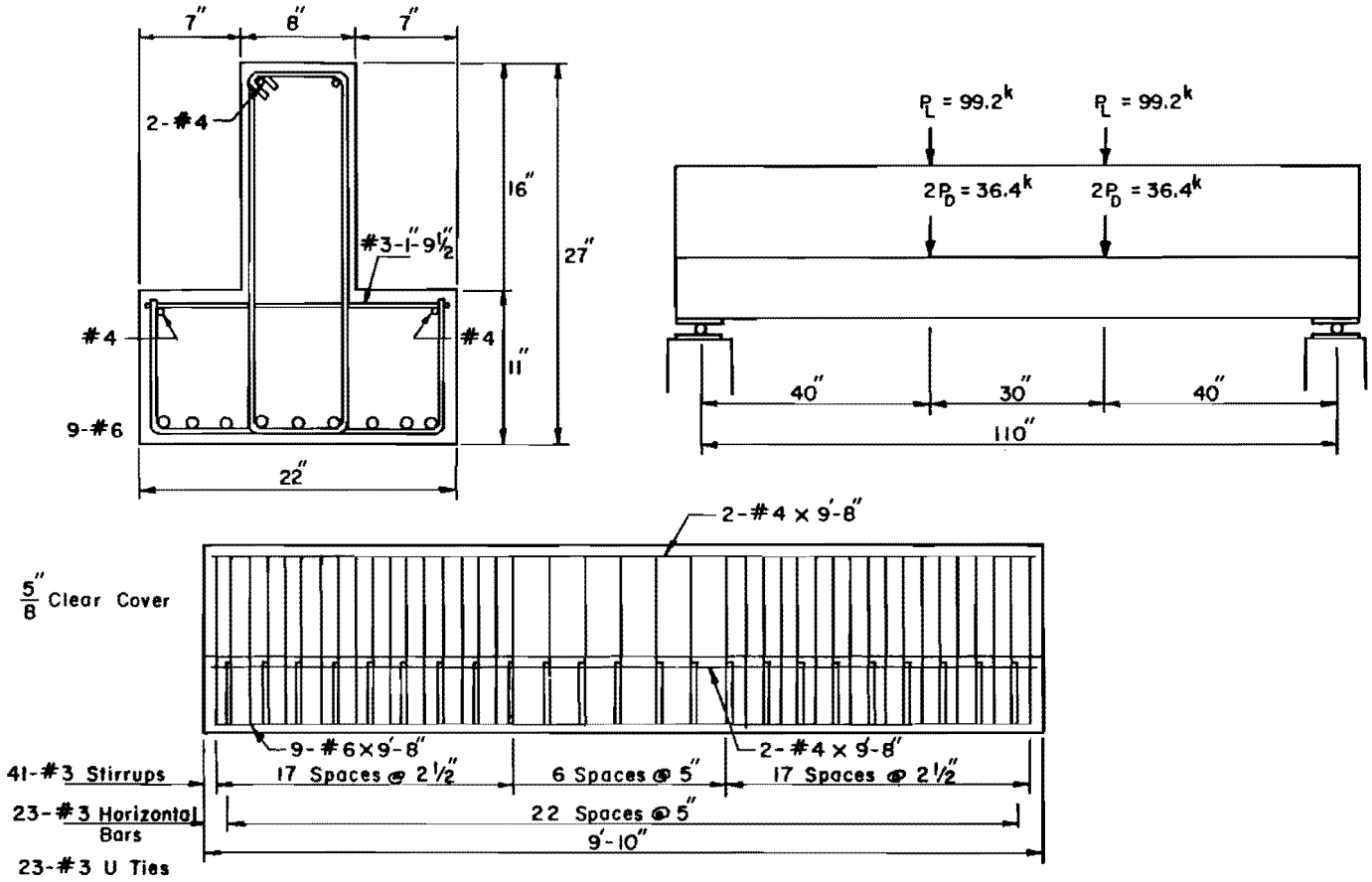

Fig. 2.2 Dimensions, reinforcement, and predicted maximum loads for Beams BMS2 and BMSP2

TABLE 2.1 PROPERTIES OF SPECIMENS

(a)

Specimen	Av. breadth of web in constant moment region b_w in.	Av. width of flange in constant moment region b_f in.	Av. thickness of flange in constant moment region t_f in.	Av. depth of web in constant moment region d_w in.	Area of tensile steel A_s $in.^2$
BMS1	8.25	22.125	6.094	16.156	1.77
BMSP1	9.05	22.188	6.188	16.906	1.77
BMS2	8.313	22.292	11.135	16.281	3.93
BMSP2	7.875	21.875	11.078	16.563	3.93

Span of all beams = 110 in.

(b)

Specimen	Av. yield stress for tension steel f_y, ksi	f'_c		f_r	
		For flange psi	For web psi	For flange psi	For web psi
BMS1	65.5	4846	4846	515	515
BMSP1	65.5	5540	4004	612	455
BMS2	60.7	5208	5208	553	553
BMSP2	60.7	5173	5540	553	612

were used to provide the bracket reinforcement. The details of reinforcement for BMS1 and BMSP1 are shown in Fig. 2.1.

Specimens BMS2 and BMSP2 (flange thickness = 11 in.) consisted of nine #6 Grade 60 longitudinal bars as flexural reinforcement (area = 3.93 sq. in.). Two #4 bars were placed near the top of the web and two #4 near the top of the flange, in order to hold the stirrups in place during casting. The shear reinforcement for the flange was twenty-three #3 U-shaped bars at 5 in. center-to-center, while the web (shear) reinforcement was forty-one #3 closed stirrups (2 legs) with a spacing of 5 in. on center, between the load points and 2-1/2 in. for the rest of the span. Twenty-three #3 straight bars at 5 in. spacing were provided near the top of the flange to take care of bracket action of the projected flange portion. Figure 2.2 shows the details of reinforcement for specimens BMS2 and BMSP2.

2.2.4 Method of Construction. Steel Cage. Grade 60 deformed bars were used. The bars were cut to size and the stirrups and U-bars were bent according to the standard specifications for bending. Stirrups and U-bars were tied to the main reinforcement with steel ties in accordance with Figs. 2.1 and 2.2. Transverse 22 in. long, #3 bars were welded to the U-bars so that the two formed a closed stirrup to provide shear reinforcement for the flange section. The weld also helped in anchoring the 22 in. bars which acted as bracket flexural reinforcement.

Forms. Forms were made with braced 3/4 in. thick plywood boards, cut to size and joined firmly together by 1-1/2 in. x 3 in. wooden framework. Three different sets of forms were used. One for control specimens and the other two for the flanges and webs of the stage-cast specimens, respectively. The flange thickness of forms could be changed from 6 in. to 11 in. by replacing the 6 in. wide plywood sides with 11 in. wide ones. One-quarter inch holes, 2 in. center-to-center along two vertical lines 20 in. apart (10 in. on either side of the midspan) were drilled in the sides of the forms. The first hole on the web was 2 in. below the top fiber and that on

the flange was 1 in. below the top of the flange. Tamp pins used for installing strain meters were held against the sides of forms by means of bolts inserted through these holes. Two 1 in. diameter, 12 in. long tubes were placed at the ends of the control specimens along their centroidal axis. These holes were used to lift the specimens. Stage-cast specimens, however, were lifted by the web reinforcement.

Forms used for casting the web of stage-cast specimens consisted of two pieces of plywood 16 in. wide and more than 10 ft. long. The lower edges of the plywood were lined with polystyrene foam of varying thickness at all sections equal to the actual deflection of the flange along the length. The webs of stage-cast specimens were, therefore, deeper at midspan than at the ends.

Casting. Control specimens were usually cast simultaneously with the flange of stage-cast specimens so that the same mix was used in the two. Steel cages were placed in proper position in the forms and concrete was poured from the top. Twenty cylinders--ten for control specimens and ten for flange of stage-cast specimens--were cast simultaneously. Vibrators were used to keep consolidate fresh concrete for the specimens as well as for the cylinders. Inverted T-beam control specimens were cast upside down (flange on top) to facilitate proper placement of concrete in the forms. Stage-cast specimens, however, were cast in an upright position, with the web reinforcement extending outside on top. Forms were usually removed two days after casting and the specimens were moist cured for two weeks.

Forming Stage-cast Web Segments. The flanges of stage-cast specimens were loaded at two sections 40 in. from either support, until the stress in tension steel reached 45 ksi. This load was maintained for about a week by means of spring assemblies. Details of the loading procedure are given in Sec. 2.3. Forms were inserted in the space between the web reinforcement and the spring assemblies. Eight inch long spacers were tied to web reinforcement to control the width of the web. Web forms were clamped against the spacers and the end sections. Forms were also clamped against the flange surface to

prevent leakage of water from concrete, as shown in Fig. 2.3. Tamp pins were bolted to the sides of the form and concrete was poured from the top. Ten cylinders were cast. Vibrators were used during casting of the web and the cylinders. Flange load was maintained during casting. Forms could not be removed after two days because the bolts holding the tamp pins were behind the springs and could not be taken out in the presence of the springs. The forms, therefore, were removed after five days by transferring the sustained load from the flange to the web in order to remove the springs. Spring assemblies were again placed on the flanges immediately after the removal of forms and installation of strain meters on the web, and the load was transferred back to the springs. The web was cured for one more week and the beam was tested to failure thereafter.

2.2.5 Concrete Mix. The concrete mix was designed according to Texas Highway specifications for compressive strength f'_c of 4000 to 5000 psi. Maximum size of the aggregate was 3/4 in. Readymix concrete was used with a desired slump of 4 in. High early strength cement was used only in webs of stage-cast specimens.

Listed below are typical proportions of the materials used per cubic yard of concrete:

Cement (Type I or Type III*)	564 lbs
Coarse Aggregate	1820 lbs
Fine Aggregate	1450 lbs
Water	230 lbs
Septair	2 oz
Airsene	30 oz

*Type I cement was used for control specimens and flange of stage-cast specimens. Type III was used in the web of stage-cast specimens.

Vibrators were used during casting of the specimens. Forms for the control specimens and the flange of stage-cast specimens were usually removed two days after casting, and those for webs of stage-cast specimens five days after casting. All specimens were cured for two weeks.

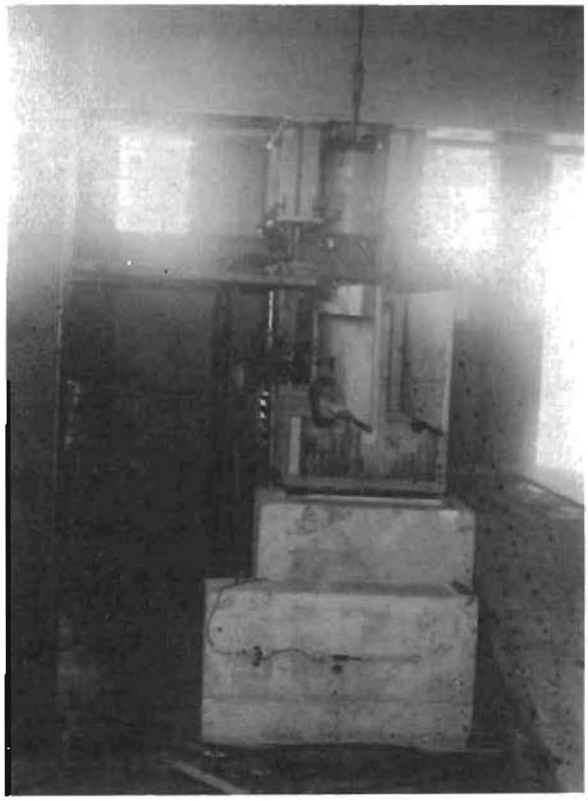

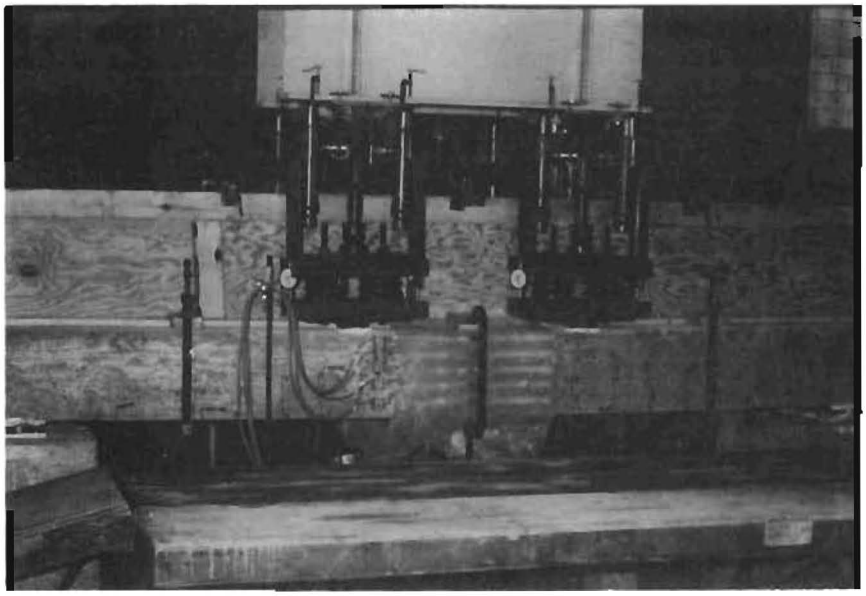

Fig. 2.3 Forming stage-cast web segments

Although the concrete mixes were designed for a cylindrical compressive strength of about 4000 psi, the average compressive strength of the cylinders was usually found to be more than 5000 psi. In the mix for beam BMS2 and the flange of BMSP2, 5.45 gallons of water was added per sack of cement by mistake, instead of 5.00 per sack. The slump was found to be 8.5 in. in this case, but the average compressive strength (f'_c) of the cylinders was still found to be 5208 psi when BMS2 was tested.

2.2.6 Steel Properties. Grade 60 steel was used in all beams to provide main (flexural) reinforcement as well as shear and bracket reinforcement. A typical stress-strain curve of the steel is shown in Fig. 2.4. The average yield strength of four #3 bars was 67.0 ksi, that of four #4 bars was 65.5 ksi, and that of four #6 bars was 60.7 ksi. The yield strength was established based on an 0.2 percent offset.

2.3 Loading

2.3.1 Location of Load Points. Loads were applied at two symmetrical points 40 in. from the supports in order to make the shear span "a" approximately twice the depth (d = 20.75 in.) of beams with a 6 in. flange. The simply supported span was 110 in. which made the constant moment region between the loads equal to 30 in. The same span and load points were adopted for 11 in. flange sections.

Flange Load Points. Flanges were loaded at four points in all--two at each loading section, as shown in Fig. 2.5. Loads were applied by spring assemblies (described in Sec. 2.3.3) placed on 4 in. x 4 in. x 1 in. steel loading plates. The load points were 5 in. from the face of the web (i.e., 9 in. from the axis of the beam). Equal loads were applied at the four load points at all load stages, in order to avoid torsional moments.

Web Load Points. Loads on top of the webs were applied equally at two points--load points 5 and 6 in Fig. 2.5. Steel loading plates 6 in. x 6 in. x 1 in. were fixed at the load points by means

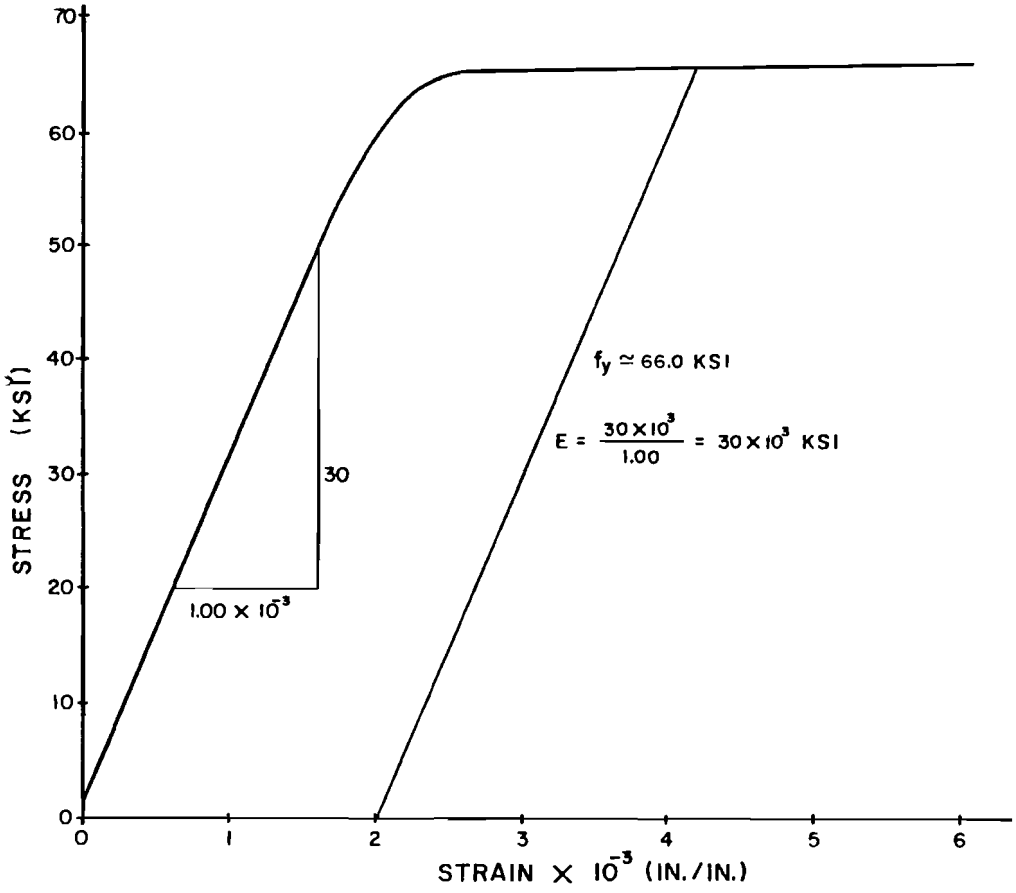

Fig. 2.4 Typical stress-strain curve for steel

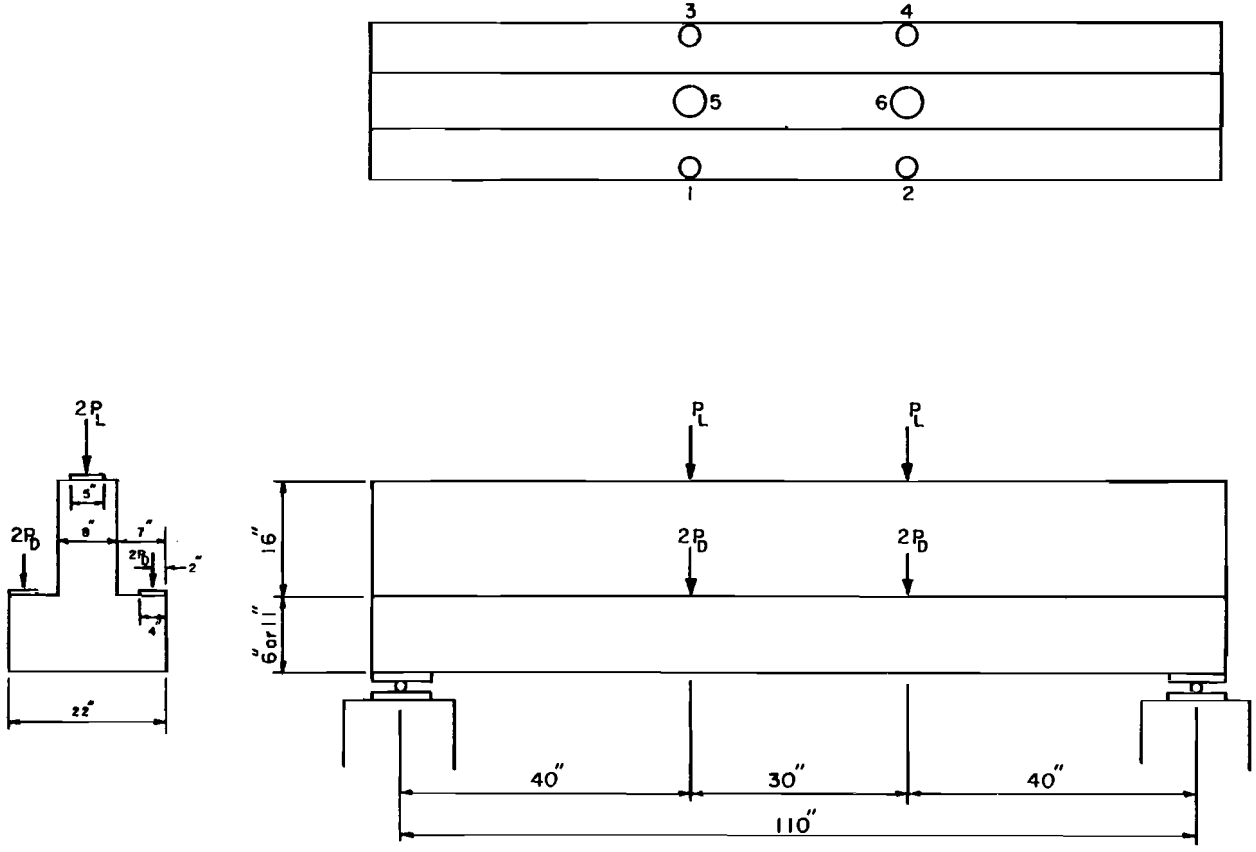

Fig. 2.5 Locations of load points

of hydrocement. Loads were applied by two 100 ton rams described in Sec. 2.3.3.

2.3.2 Loading Sequence

2.3.2.1 Loading Sequence for Stage-cast Specimens. Flange Load. The flange of stage-cast specimens was loaded prior to casting the web. Loads were applied symmetrically to the axis of the beam, in increments causing an increase of about 5 ksi in tensile steel stress per load increment, until the calculated stress in the tension steel reached 45 ksi. This load was maintained for about two weeks (one week before casting the web and about five days after it). The springs were then removed for a day by applying an equivalent amount of load on top of the web in order to remove the forms and to install the strain meters as described in Sec. 2.2.4. The web loads were removed and the springs were loaded to the same magnitude again. This load was maintained for one more week and the web was loaded thereafter.

For a 6 in. flange, the load producing 45 ksi of steel stress was 4.05 kips at each of the four load points (load points 1 through 4 in Fig. 2.5). This load was achieved in eight load stages by increasing 0.5 kip per load point at every load stage from a load of 1.0 kip per load point at load stage 1 to 3.5 kips per load point at load stage 6, and then reducing the load increment by half for the last two load stages.

For an 11 in. flange a load of 18.2 kips per load point was applied in nine load stages to produce a tensile stress of 45 ksi in the steel. The increment for each load stage was 2 kips at each load point.

Web Load. Loads were equally applied on top of the web at load points 5 and 6 (see Fig. 2.5), when the compressive strength of the web concrete became close to that of the corresponding control specimen on the day of the test. Flange loads were maintained during the loading of the web. Load equal to that predicted at ultimate was applied in ten load stages with equal increments of about 10 percent

of the predicted load. Hence, the load increment for BMSP1 was 5 kips per load point and that for BMSP2 was 10 kips per load point. Predicted loads for beams are shown in Figs. 2.1 and 2.2. Load increment was reduced near the predicted load so that three to five readings could be taken near the actual failure. The total number of load stages for web loading was 17 for BMSP1 and 15 for BMSP2.

2.3.2.2 Loading Sequence for Control Specimens. Flange Load. The flange of the control specimen also was loaded before loading the web. The magnitude of the flange load was the same as that for stage-cast specimens. However, the same load was achieved in a fewer number of load stages. Three load stages (instead of eight) with equal increments for BMS1 and four (instead of nine) with equal increments for BMS2 were adopted. Flange load for control specimens was not sustained for long periods and web loads were applied on the following day.

Web Load. Web loads were applied in less than a day after the loading of the flange. Load increments the same as those for corresponding stage-cast specimens were adopted. Flange loads were maintained throughout (as in the case of stage-cast specimens). Hence, the procedure for web loading of control specimens was exactly similar to that for the corresponding stage-cast ones.

2.3.3 Loading Equipment and Load Monitoring

2.3.3.1 For Flange. Spring assemblies and mechanical jacks were used for loading the flanges so that a fairly constant load could be maintained on the flanges. The entire loading system is shown in Fig. 2.6.

Each spring assembly consisted of two helical springs, approximately 5-1/2 in. in diameter, placed in between two 7 in. x 9.8 lb. channels. All four spring assemblies were calibrated by applying known magnitudes of load through a loading machine and by measuring the resulting shortening of springs by means of dial gages. The spring constant (or spring factor) for all the assemblies was close to 8 kips/in. The spring assemblies were calibrated up to a load of

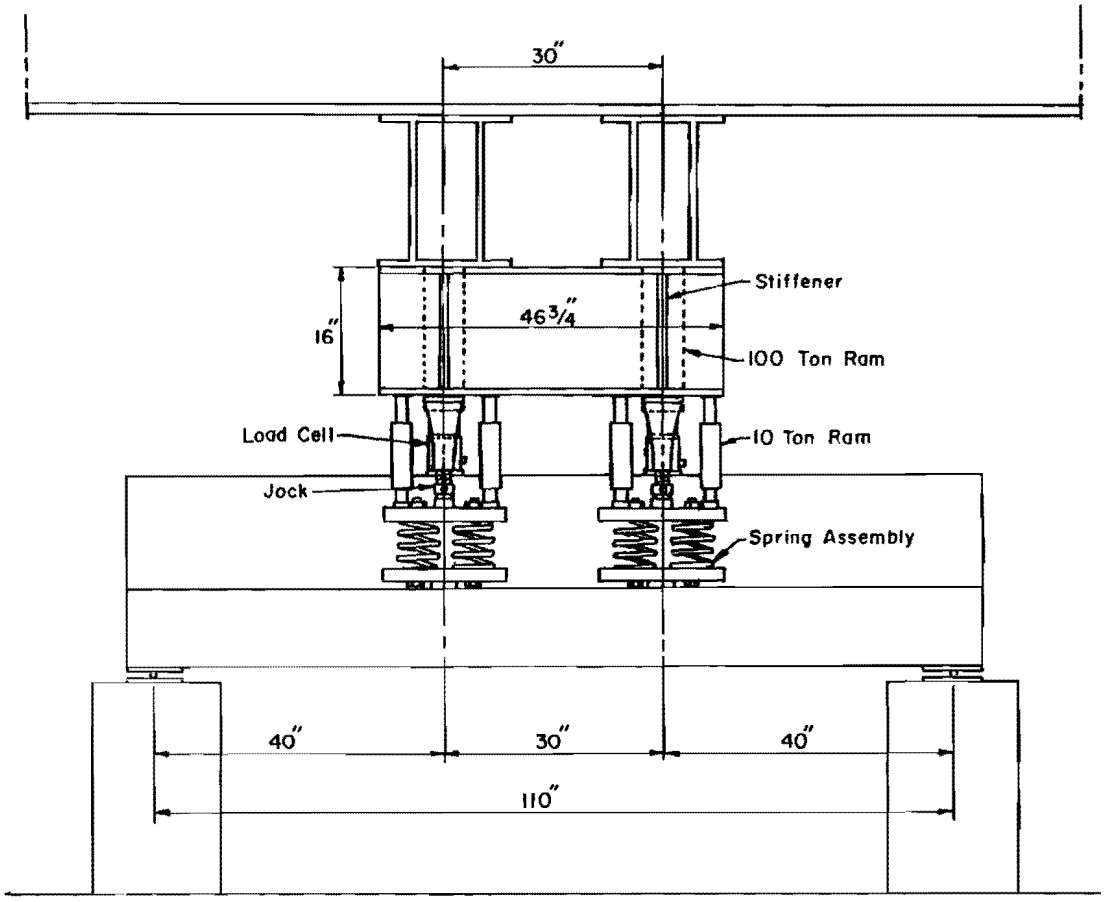

Fig. 2.6 Loading system

20 kips and were found to behave linearly up to a load of about 16 kips. Since a load of 18.2 kips per spring assembly was desired for BMS2 and BMSP2, the load during the test was achieved by using the actual readings recorded at the time of calibration rather than the average calibration.

In order to apply a desired load with the help of spring assemblies, the required amount of compression of the springs was calculated using the average calibration (or spring factor). If the load was in the nonlinear region (i.e., greater than 16 kips), the actual reading from calibration data was used. This quantity was added to dial gage readings to obtain the required dial gage readings for the load. The springs were then loaded until the average of the actual dial gage readings was equal to that of the required ones. Sustained loads were maintained by noting the sum of the dial gage readings for each assembly and adjusting the springs every day by making the sum of the dial gage readings the same as the original one.

Mechanical jacks were used to compress the springs. Two 10-ton rams were used per spring assembly to assist the mechanical jacks in case it was difficult to turn the jacks due to heavy loads. The rams were, however, removed and the total load was applied through the jacks when the load was to be sustained.

Table 2.2 shows one set of readings obtained during the calibration of spring assembly No. 1. Two sets of such readings were used to compute the spring factor for each of the four assemblies. Figure 2.7 shows calibration curves for the spring assemblies.

2.3.3.2 For Web. Two 100-ton rams were used to load the web, as shown in Fig. 2.6. The maximum expected load was 99.2 kips at each load point.

Load cells were calibrated before the tests began. Another set of calibrations was obtained after three tests. Figure 2.8 shows one set of calibration curves for the load cells.

TABLE 2.2 CALIBRATION DATA FOR SPRING ASSEMBLY No. 1

Ave. spring factor (based on Load Nos. 2 through 15) = 8.220 k-in.

Load No.	Load (lb.)	Dial Gage Reading 1 (in.)	Dial Gage Reading 2 (in.)	Average Shortening (in.)	Spring Factor (k-in.)	Remarks
0	0	0.1750	0.0395	0		
1	1300	0.3625	0.2410	0.1945	7.198	
2	2280	0.4720	0.3730	0.1208	8.113	
3	3230	0.5850	0.4920	0.1160	8.190	
4	4210	0.7030	0.6170	0.1215	8.066	
5	5200	0.8205	0.7400	0.1203	8.229	
		0.1735				Reset
6	6200	0.2980	0.1450	0.1238	8.078	
7	7260	0.4230	0.2755	0.1278	9.294	
8	8200	0.5365	0.3935	0.1158	8.117	
9	9110	0.6475	0.5045	0.1110	8.198	
10	10070	0.7640	0.6225	0.1173	8.184	
11	11160	0.8960	0.7570	0.1333	8.177	
		0.1165	0.0445			Reset
12	12170	0.2430	0.1665	0.1243	8.126	
13	13150	0.3590	0.2845	0.1170	8.376	
14	14150	0.4770	0.4060	0.1198	8.347	
15	15060	0.5840	0.5110	0.1060	8.585	Cumulative shortening from 2.28k to 18.14k = 1.9057 in. Nonlinear
16	16130	0.7070	0.6350	0.1235	8.664	
17	17140	0.8195	0.7515	0.1145	8.821	
18	18140	0.9345	0.8640	0.1138	8.787	
		0.6375	0.5075			Reset
19	19230	0.7470	0.6160	0.1090	9.083	
20	20340	0.8460	0.7190	0.1010	10.991	

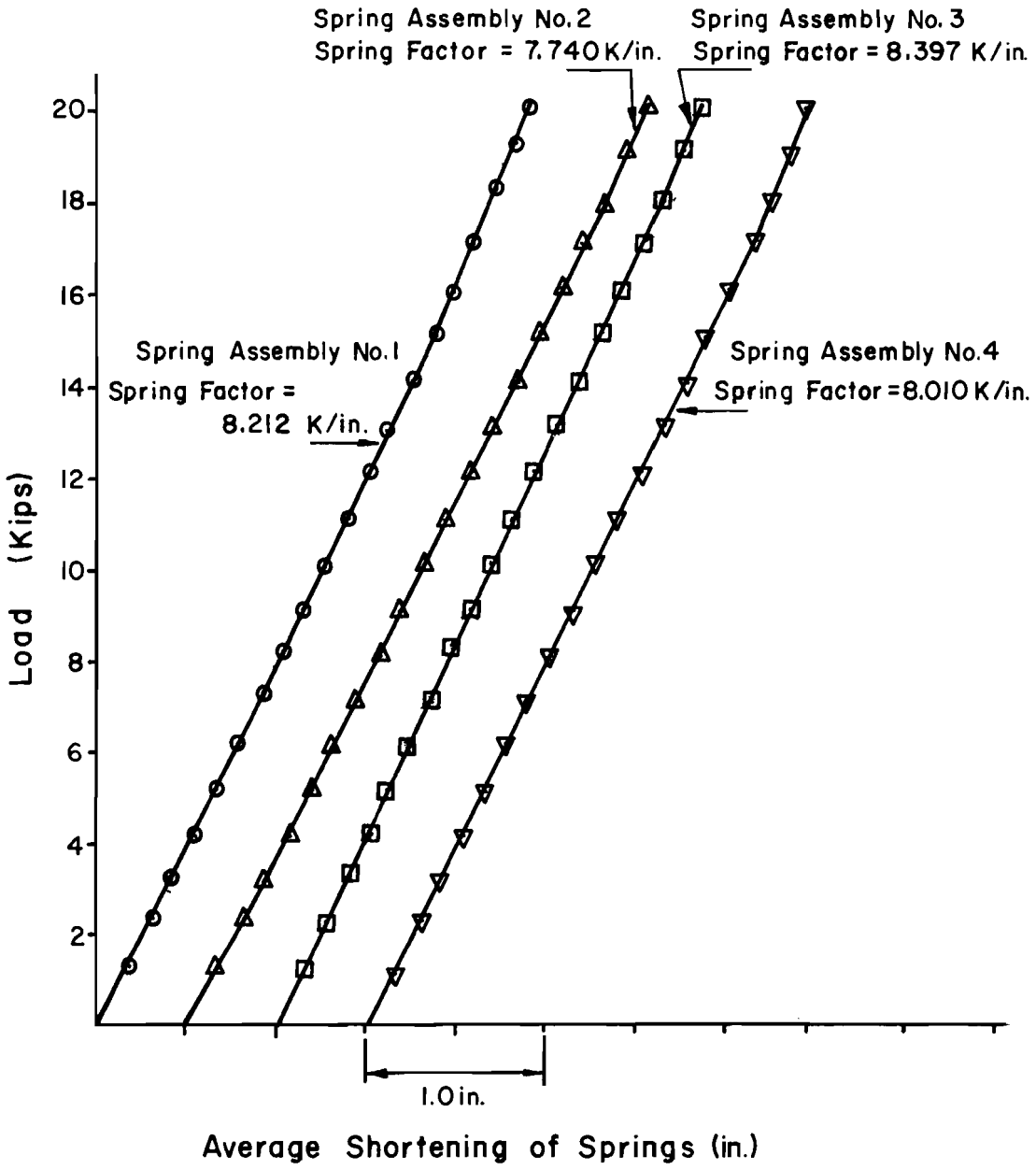

Fig. 2.7 Calibration curves for spring assemblies

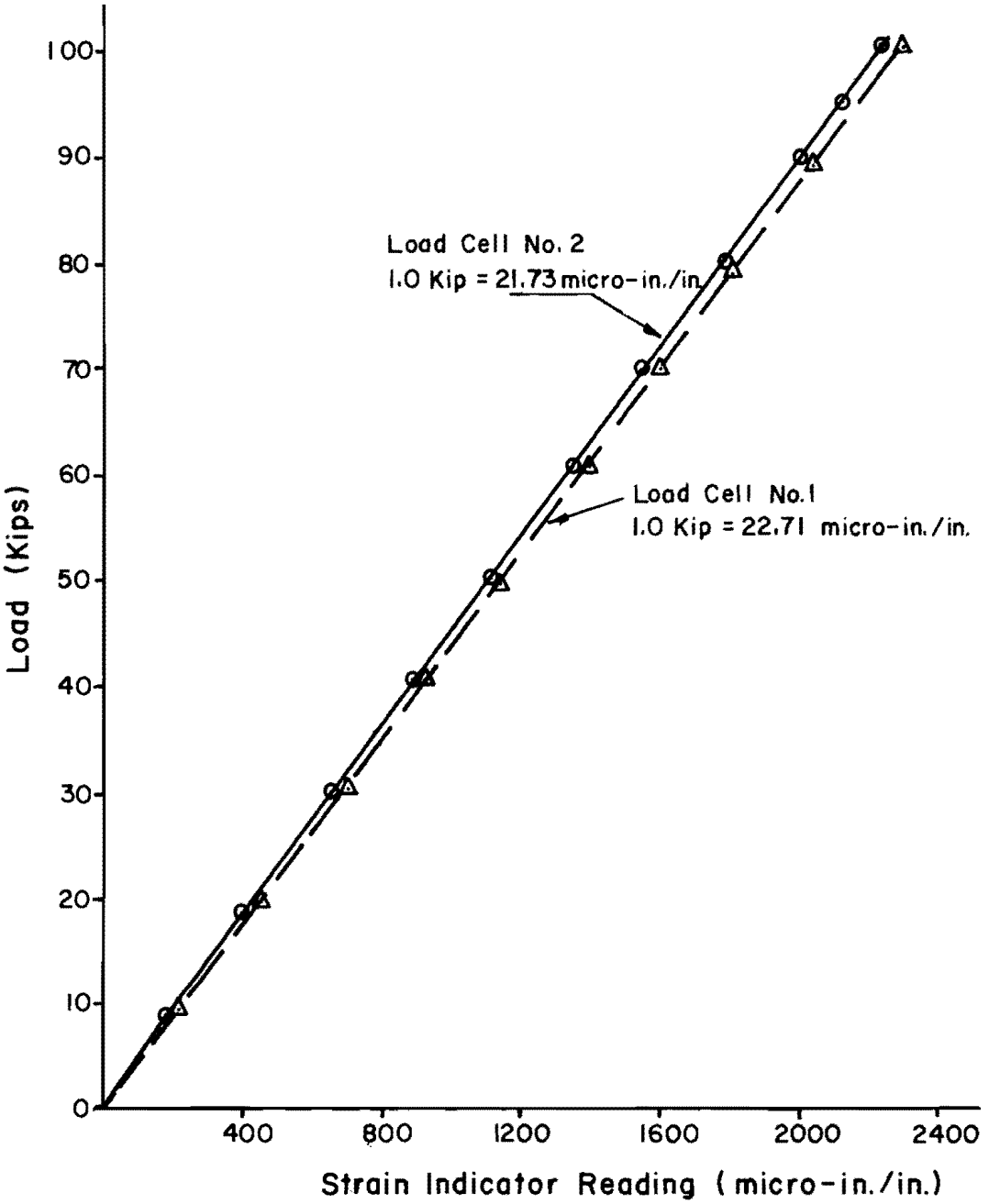

Fig. 2.8 Typical calibration curves for load cells

Desired load was achieved during the test by computing the amount of strain that will be produced in each load cell due to the load. Load cell calibrations were used to compute this strain. Load was applied until the actual strain in the load cells reached the computed one. The magnitude of load was verified by calculating the load by pressure transducer readings and pressure gage readings.

2.4 Measurements

2.4.1 Flexural Strains. A simple strain measuring instrument called a strain meter was built in the laboratory. Figure 2.9 shows the essential features and dimensions of a strain meter. A similar though smaller instrument was first made and successfully used at the University of Missouri at Columbia.[5]

Each strain meter was made from three 8 in. x 3/4 in. x 1/16 in. aluminum strips (or plates) and two 1-1/2 in. x 1 in. x 3/4 in. aluminum blocks. Holes 3/16 in. in diameter were drilled in the aluminum strips and the blocks to join them together by screws. Four SR-4 strain gages (two on each face) were mounted at the center of the middle strip. The gage length of each strain meter was 20 in. and the overall length 21 in., as shown in Fig. 2.9.

The functioning of a strain meter is simple. It can be attached to the surface of a body whose surface strains are to be measured, by means of bolts passing through the 1/4 in. holes in the end strips (see Fig. 2.9). Any surface strain produced in the body will increase or decrease the space between the two 1/4 in. holes, thus causing the middle strip of the strain meter to bend. The curvature of the middle strip can be measured by the SR-4 gages by connecting the gages to a strain indicator. The strain in the specimen can be computed from the difference between the strain indicator readings, using a strain meter factor obtained by calibrating the strain meter.

Strain meters were calibrated on a device shown in Fig. 2.10. The strain meter to be calibrated was mounted on the calibrator in

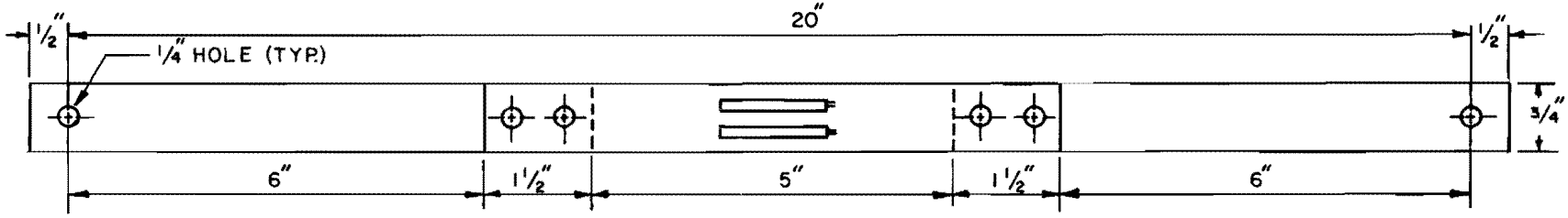

TOP VIEW

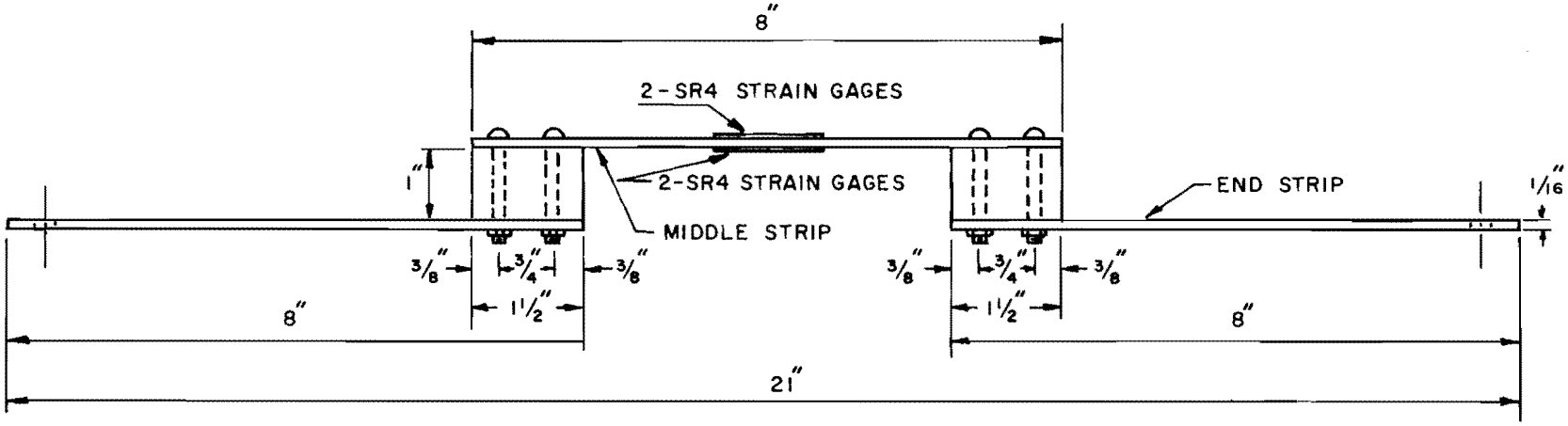

SIDE VIEW

Fig. 2.9 Strain meter

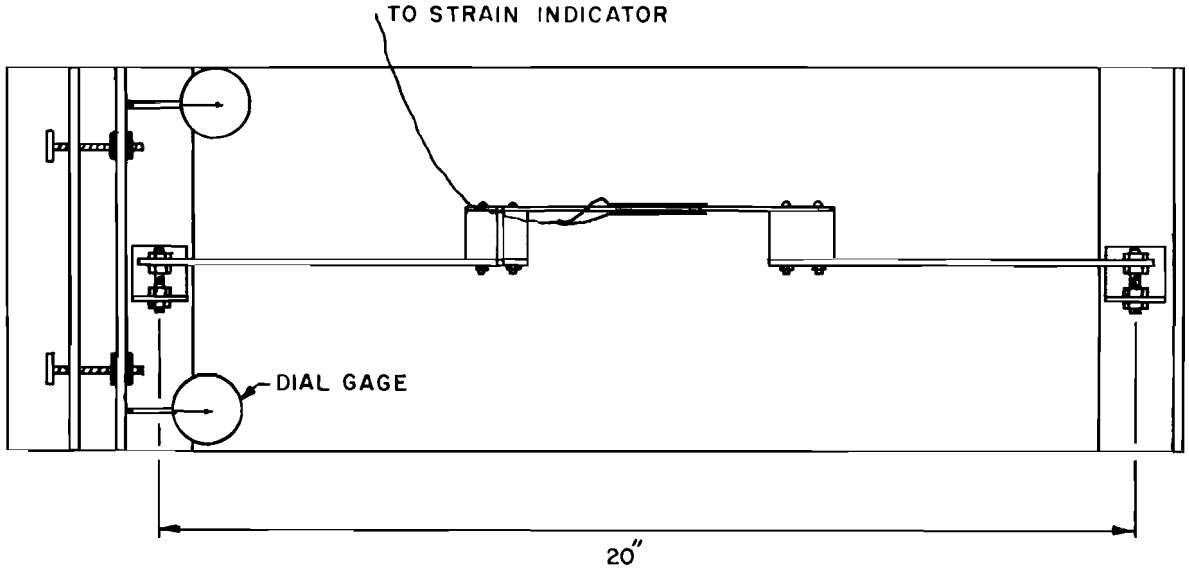

Fig. 2.10 Strain meter calibrator

the same position as it would be on the specimen. Bolt connections similar to those used during tests were used for connecting the strain meter to the calibrator (see Fig. 2.10). In order to calibrate the strain meter was elongated or shortened by a specific amount (measured by dial gages) and the change in reading of SR-4 gages was recorded with the help of a strain indicator. It was observed that the behavior of the strain meter was nonlinear under compressive strains, but quite linear under tensile strains not exceeding 0.008 in./in. Due to nonlinear behavior in compression, the strain meters required to measure compression were pretensioned (elongated by a desired amount) before mounting. Hence, the strain meters actually measured compression as a decrease in tension. The strain meter closest to the extreme compression fiber was pretensioned to a tensile strain of 0.005 in./in. Table 2.3 shows one set of readings obtained during the calibration of strain meter SM1. Two sets of such readings were used to compute the average strain meter factor for each strain meter. Plots in Fig. 2.11 illustrate the linear behavior of strain meters SM1 and SM2 in tension. The strain meter factor for most of the strain meters was close to 5×10^{5} per unit strain; i.e., the least count of the strain meters was 2 microstrain (2×10^{-6} in./in. strain).

Strain meters were installed on the sides of the specimens. Twenty-four strain meters (twelve on each side) were placed on specimens BMS2 and BMSP2, and twenty (ten on each side) on BMS1 and BMSP1. Fourteen strain meters (seven on each side) were placed on web sides in all cases. Strain meters were spaced at 2 in. vertically. Strain meters were bolted to tamp pins which were placed at desired locations along the sides of the specimens at the time of casting. Figure 2.12 shows the desired locations of tamp pins for specimens of both sizes. It also shows the top strain meter installed at its desired location. Due to imperfections in forms, the actual gage lengths and locations of strain meters were slightly different from the desired ones. Table 2.4 shows the actual gage lengths and locations of strain meters attached to BMS1.

TABLE 2.3 CALIBRATION DATA FOR STRAIN METER

Gage Factor Setting = 2.00
Gage Length = 20.0 in.

Strain Meter No. SM1
Tension Test No. 1 of 2
Date: July 3, 1975

Dial Gage Reading	Displacement $\times 10^{-3}$ in.	Unit Strain $\times 10^{-4}$ in./in.	Strain Indicator Reading (Stretching)	Strain Indicator Reading (Releasing)	Average Increment	Increment Sum
0	0	0	0	+6	0	0
90	10	5	232	238	232	232
80	20	10	454	467	226	458
70	30	15	678	692	224	682
60	40	20	912	925	234	916
50	50	25	1146	1057	232	1148
40	60	30	1380	1394	236	1384
30	70	35	1616	1631	240	1624
20	80	40	1854	1865	233	1857
10	90	45	2101	2112	247	2104
0	100	50	2350	2350	243	2347

S.M. factor = (Sum of Average Increment)/(Sum of Unit Strain)

$= 4.637 \times 10^{5}$ per unit strain

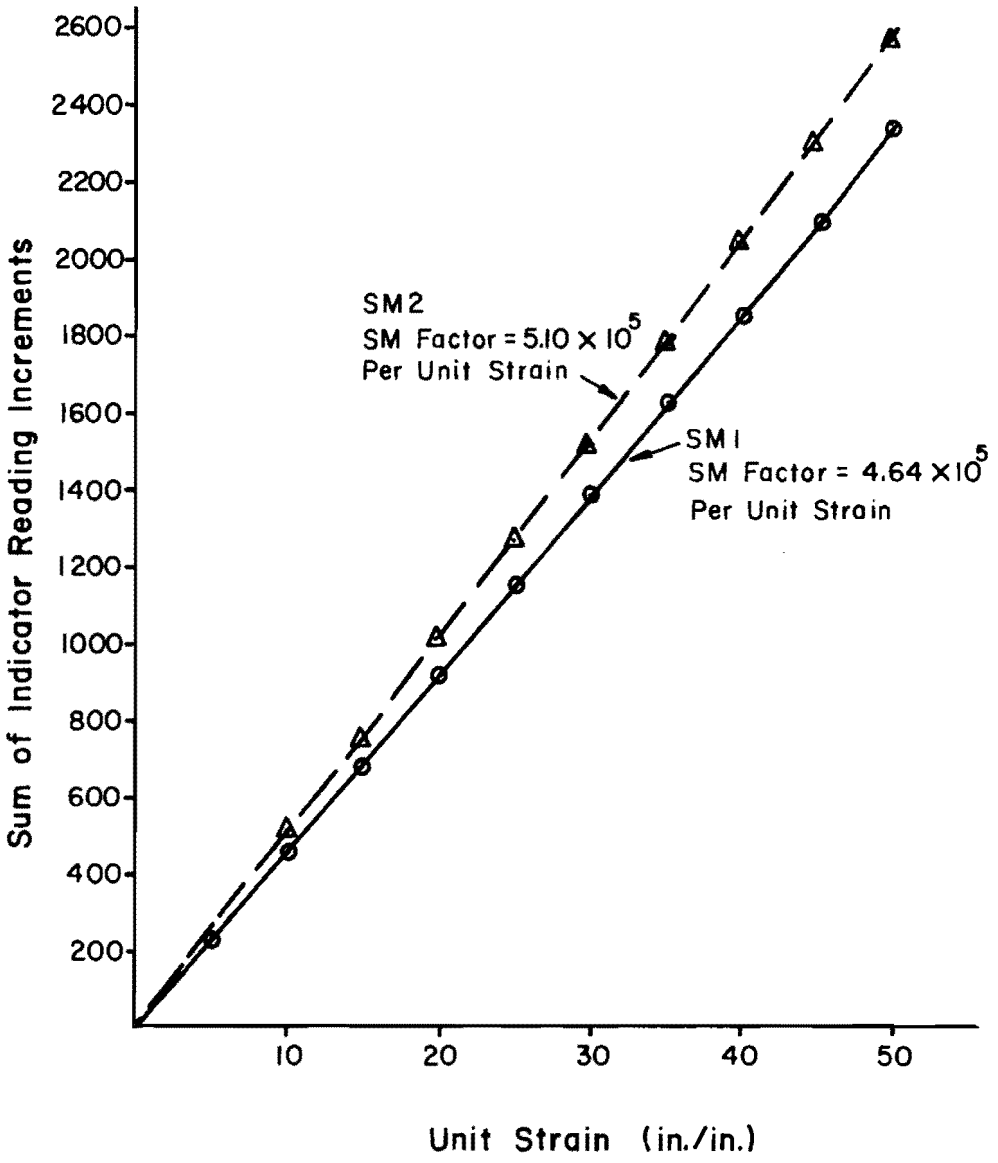

Fig. 2.11 Typical calibration curves for strain meters

TABLE 2.4 ACTUAL LOCATIONS AND GAGE LENGTHS OF STRAIN METERS ON BMS1

(a) Strain Meters on North Face

	SM1	SM3	SM5	SM7	SM9	SM11	SM13	SM15	SM17	SM19
Gage length, in.	20.00	20.06	19.94	20.03	20.06	20.03	20.00	19.94	20.00	19.94
Distance from top at eastern tamp pin, in.	$2\frac{3}{16}$	$4\frac{3}{16}$	$6\frac{3}{16}$	$8\frac{3}{16}$	$10\frac{7}{32}$	$12\frac{3}{16}$	$14\frac{5}{32}$	$17\frac{9}{32}$	$19\frac{5}{16}$	$21\frac{1}{4}$
Distance from top at western tamp pin, in.	$2\frac{3}{32}$	$4\frac{1}{32}$	$6\frac{1}{16}$	$8\frac{3}{32}$	$10\frac{3}{32}$	12	$14\frac{1}{8}$	$17\frac{1}{4}$	$19\frac{1}{4}$	$21\frac{5}{16}$
Average, in.	2.14	4.11	6.13	8.14	10.16	12.09	14.14	17.27	19.28	21.28

(b) Strain Meters on South Face

	SM2	SM4	SM6	SM8	SM10	SM12	SM14	SM16	SM18	SM20
Gage length, in.	20.03	20.03	19.88	19.94	20.06	20.06	19.91	19.04	19.97	20.03
Distance from top at eastern tamp pin, in.	$2\frac{1}{4}$	$4\frac{1}{4}$	$6\frac{5}{32}$	$8\frac{7}{32}$	$10\frac{3}{16}$	$12\frac{3}{16}$	$14\frac{1}{4}$	$17\frac{1}{4}$	$19\frac{9}{32}$	$21\frac{9}{32}$
Distance from top at western tamp pin, in.	$2\frac{3}{16}$	$4\frac{7}{32}$	$6\frac{7}{32}$	$8\frac{3}{16}$	$10\frac{3}{16}$	$12\frac{3}{16}$	$14\frac{1}{4}$	$17\frac{7}{32}$	$19\frac{1}{4}$	$21\frac{9}{32}$
Average, in.	2.22	4.23	6.19	8.20	10.19	12.19	14.25	17.23	19.27	21.28

The advantage of using strain meters is that a strain meter measures average strains within its gage length (20 in. this case), whereas other gages measure local strains. After cracking the average strains are more useful than the local strains. A 20 in. gage length was chosen in order to include three cracks within the gage length, typically.

Since the coefficient of expansion of concrete is different from that of aluminum, a temperature correction was required. One strain meter was installed on a separate concrete block, placed near the specimen, to record the temperature effects. Strain meters were also protected from wind by a temporary paper wall. A calibrator was attached to the digital strain indicator and the switch boxes to record the effects of any fluctuation in the current or in the resistance of the wiring system.

2.4.2 Crack Size. The width of flexural cracks was usually measured at four to eight stations on each specimen. The stations were located on comparatively wide cracks so that the size of the largest crack could be measured. Width of other wide cracks was checked from time to time, and if any new crack was found to be wider than the ones being measured, a new station was established on the largest crack.

A comparator having lines of various known thicknesses was used to measure crack widths by placing these lines of known thickness over the cracks and recording the thickness of the line which just covered the crack.

2.4.3 Deflection. Deflection at midspan was measured with the help of two dial gages placed near the north and south faces of the flange at the centerline. Dial gages were capable of measuring deflections up to 0.001 in.

The dial gages were mounted vertically on stands, as shown in Fig. 2.12.

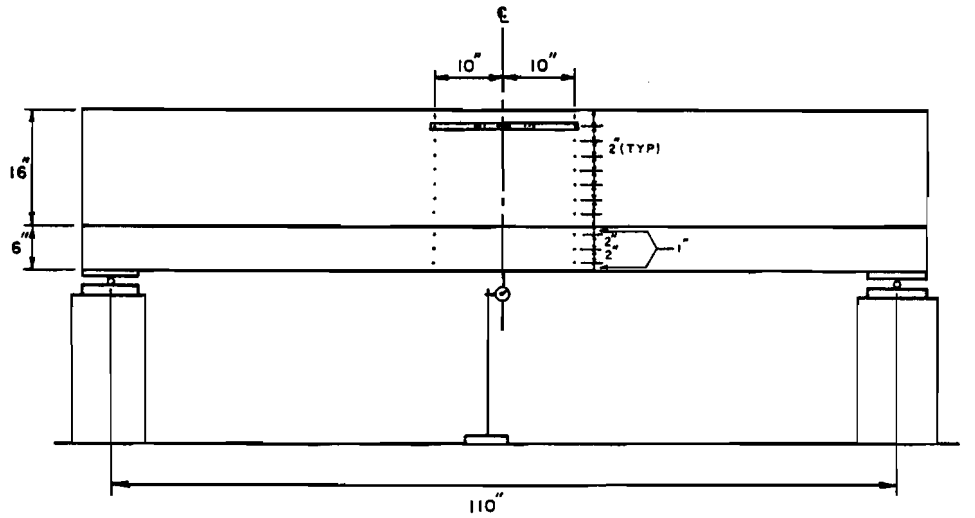

(a) BMS1 And BMSP1

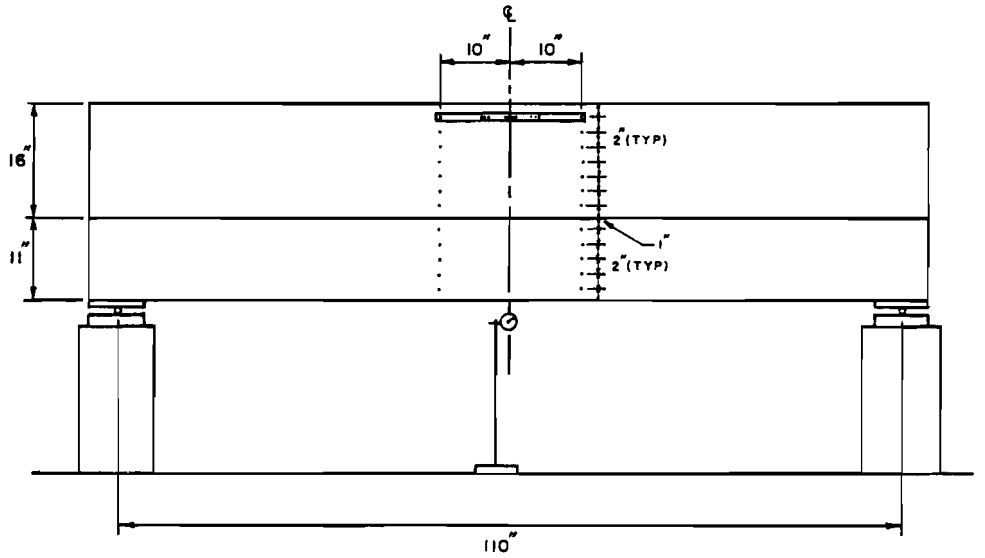

(b) BMS2 And BMSP2

Fig. 2.12 Desired locations of strain meters and dial gages

CHAPTER 3

TEST RESULTS AND DISCUSSION

Four reinforced concrete inverted T-beams were tested in order to study the flexural behavior of stage-cast inverted T-beams subjected to positive moment. The tests were intended to provide information about strain profiles, ultimate strength, ductility, stiffness, and size and propagation of cracks in stage-cast inverted T-beams as compared to monolithic T-beams of the same size and reinforcement.

Sustained loads were applied to the flanges of stage-cast beams before the webs were cast, in order to simulate the loads which are applied to such members during highway bridge construction and to provide information about the effect of creep in flange deflection and cracking.

This chapter is devoted to a presentation of test results and a discussion of the results. For analyzing the test results, the four specimens can be classified into two groups:

(1) Monolithic and Stage-cast Specimens

Specimen	Type
BMS1	Monolithic
BMS2	Monolithic
BMSP1	Stage-cast
BMSP2	Stage-cast

(2) Flange Thickness-to-Depth Ratios:

Specimen	t_f/h	d_f/d
BMS1	0.273	0.236
BMSP1	0.273	0.236
BMS2	0.407	0.387
BMSP2	0.407	0.387

Results obtained from the test program are presented in the following sections.

3.1 Strain Profiles

Surface strains were measured along both faces of the specimens with strain meters placed 2 in. on centers vertically. The strains measured as such were corrected for variations in daily temperature, the effect of which was recorded by a separate strain meter placed on a concrete block adjacent to the test beam. Figures 3.1 through 3.6 show some of the strain profiles for the test specimens. The strain profiles represent the average of the strains measured on the two faces.

In Fig. 3.3, the strain profile for BMSP1 at ultimate was plotted using the readings on only the north face because the average strain profile (shown by the broken line) implied a relative movement between the flange and web, which was not visible (as no crack appeared at the web-flange interface).

Strain profiles for flanges of both stage-cast specimens were close to a straight line, as shown in Figs. 3.2 and 3.5. The strain gradient (rate of change of strain with depth) increased slightly from top to bottom. Strain profiles for the composite section of stage-cast specimens were also basically linear (see Figs. 3.3 and 3.6), but those for control specimens were obviously nonlinear, as shown in Figs. 3.1 and 3.4. Near the yield load flexural cracks occurred along the gage-mounting anchors of control specimen BMS1. The cracks probably loosened the anchors resulting in a comparatively low recorded value of strains in the flange at yield load (see Fig. 3.1). This effect is more prominent at ultimate, due to further widening of the cracks.

3.1.1 Effect of Depth. The strain gradient was found to decrease from top to bottom for 22-in.-deep shallow flange specimens BMS1 and BMSP1, although the change in gradient was barely discernible for BMSP1. The strain gradient for 27-in.-deep thick flange specimens

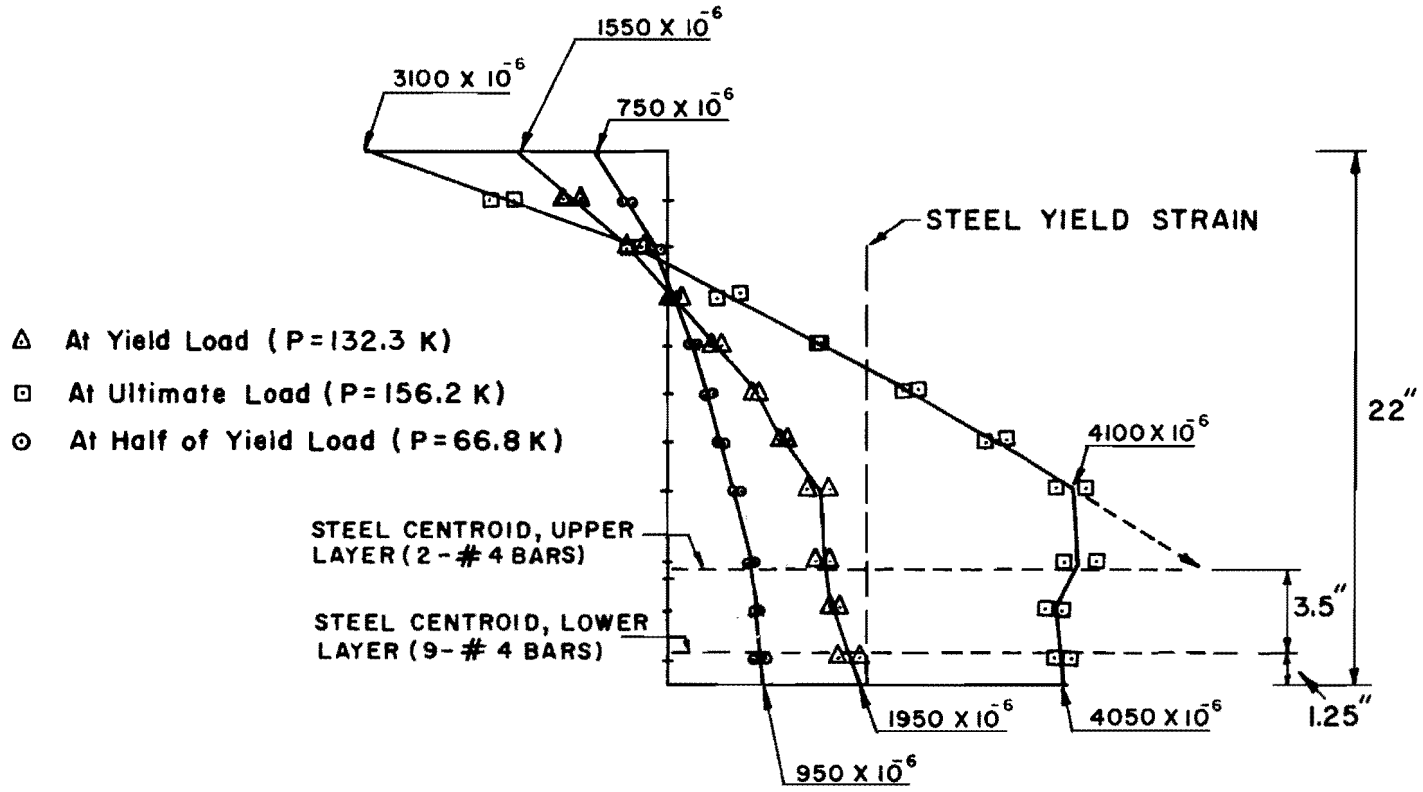

Fig. 3.1 Strain profiles for BMS1

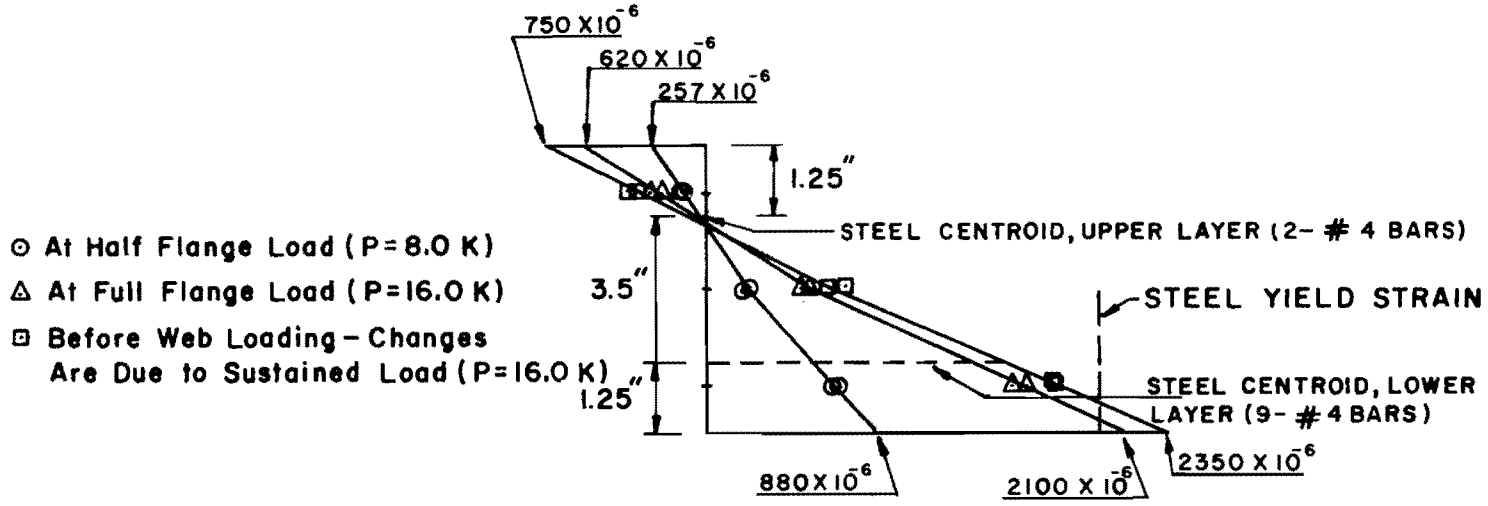

Fig. 3.2 Strain profiles for flange of BMSP1

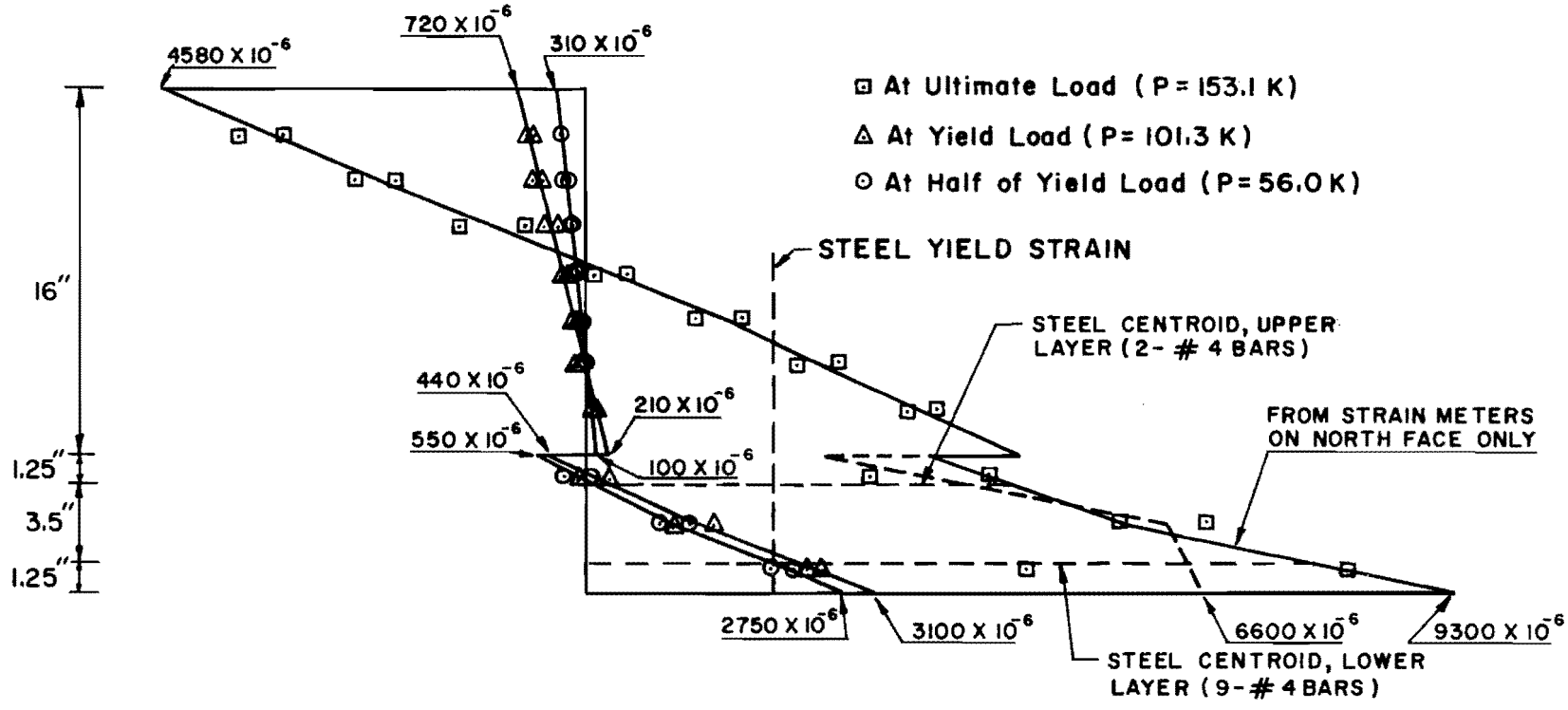

Fig. 3.3 Strain profiles for BMSP1 (composite section)

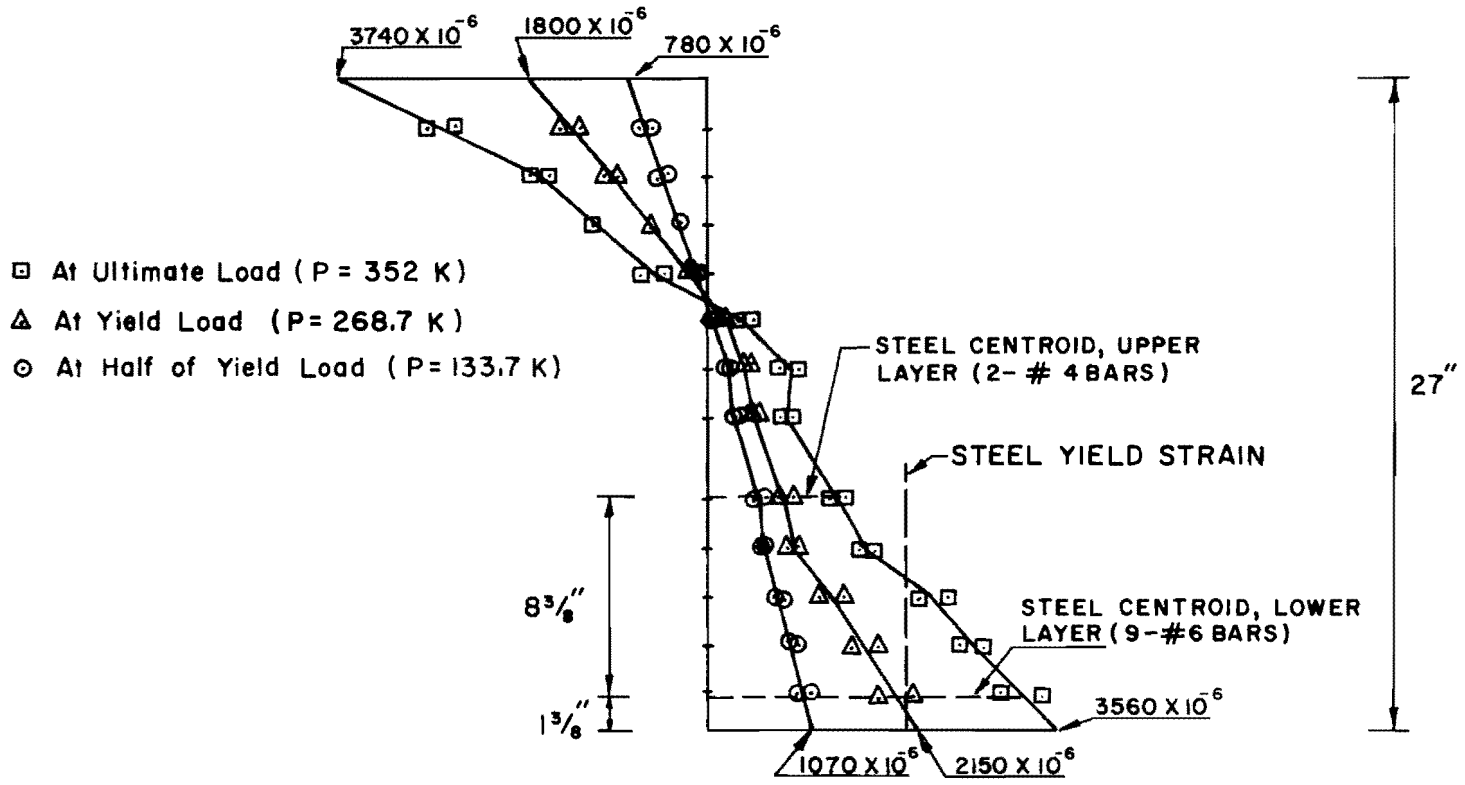

Fig. 3.4 Strain profiles for BMS2

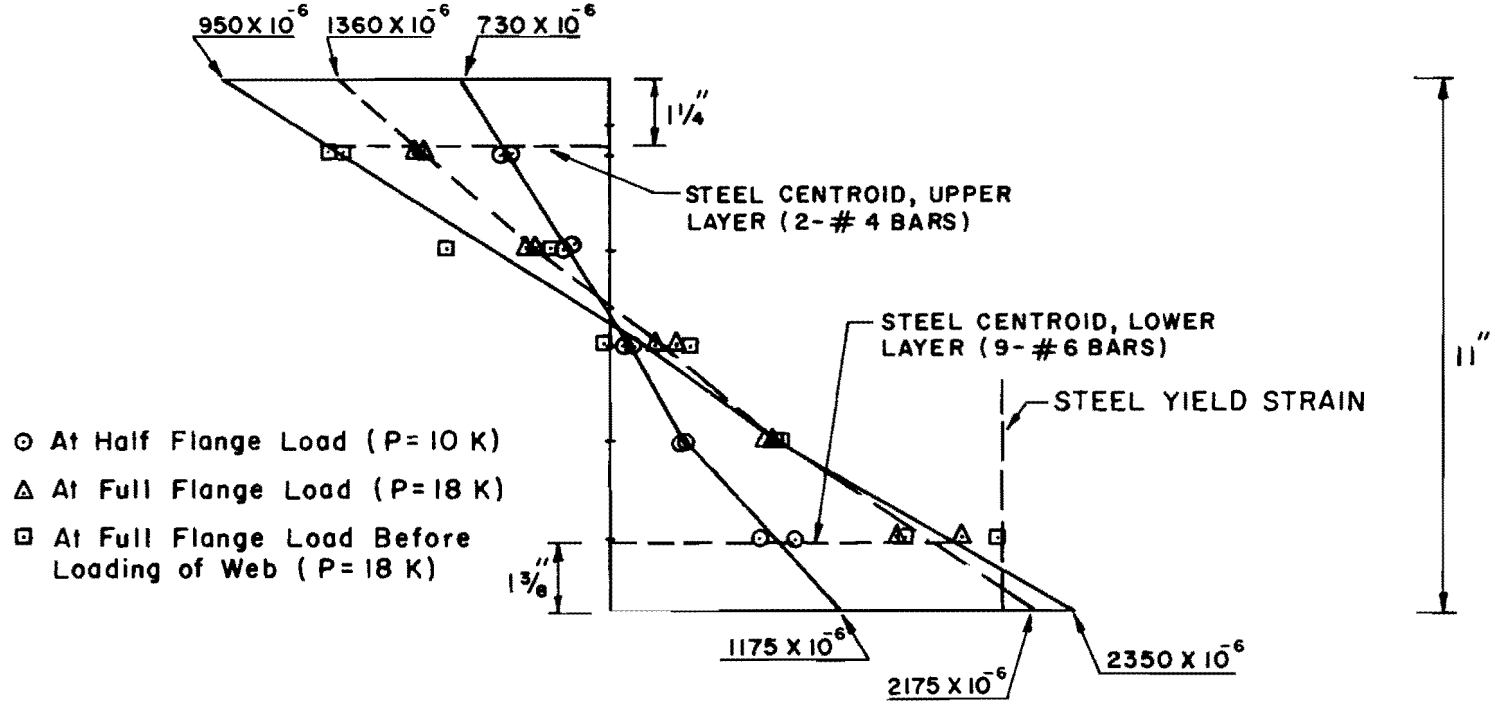

Fig. 3.5 Strain profiles for flange of BMSP2

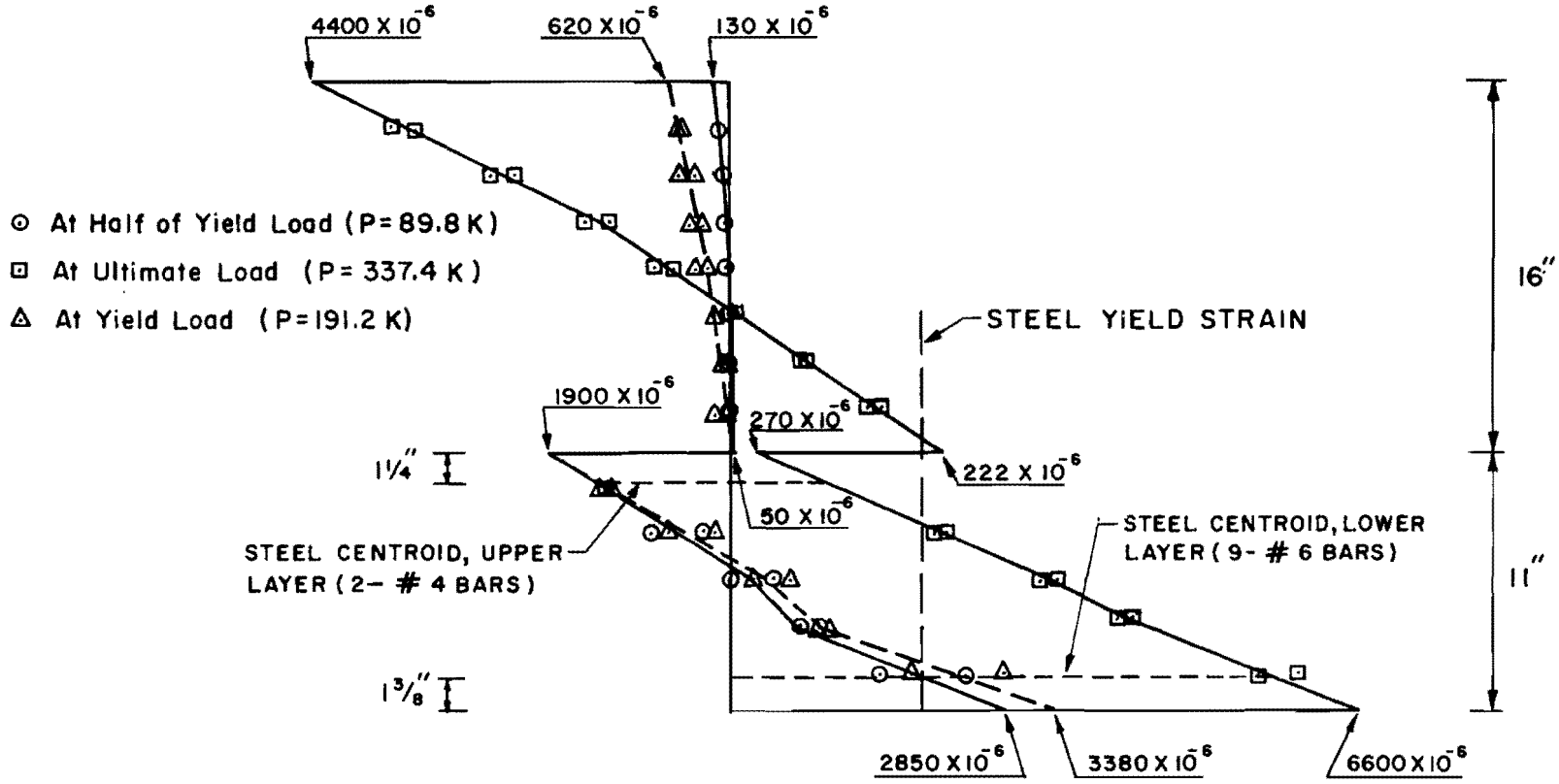

Fig. 3.6 Strain profiles for BMSP2 (composite section)

BMS2 and BMSP2 was greater near the top and bottom than at middepth. Variations of strains along the depth in the deeper beams tended toward the variation consistent with the Theory of Elasticity,[4] but the strain gradient was always greatest at the compression face of each specimen. Again the nonlinear aspects of strain gradient were less obvious for composite action in stage-cast specimen BMSP2.

3.1.2 Effect of Stage-casting. In order to compare the strain profiles of stage-cast and control specimens, the changes in strains caused by the application of web loads, neglecting any strain caused by flange loads, were plotted in Figs. 3.7 and 3.8 for stage-cast as well as control specimens at approximately equal curvatures. These illustrations show only the difference between the total strains at each "live" load and the strains that were present in the specimens at full flange preload. The curvatures selected for the plots in Figs. 3.7(b) and 3.8(b) were approximately equal to the curvatures of the respective control specimens at yield load, and those for Figs. 3.7(a) and 3.8(a) were approximately half of the above curvatures.

For shallow beams BMS1 and BMSP1, the stage-cast specimen indicated compressive strains about 0.02 percent greater than those of the control specimen. A limiting compressive strain would be more likely to occur in the stage-cast beam at superimposed web loads lower than those that could be applied to the control specimen. If the yielding of steel were a more critical parameter, the large tensile strains in the reinforcement of the stage-cast specimen caused by the preloading of the flange (to 45 ksi of steel stress) would permit steel to yield at web loads lower than those creating yield stress in the control specimen. Stage-cast specimens would, therefore, exhibit more ductile live load resistance than that of the control specimen.

The deep flange specimens indicated only slightly greater compressive strains near the neutral axis of the stage-cast specimen. The control specimen reached slightly greater changes in top surface and bottom surface strains than those observed for the stage-cast specimen

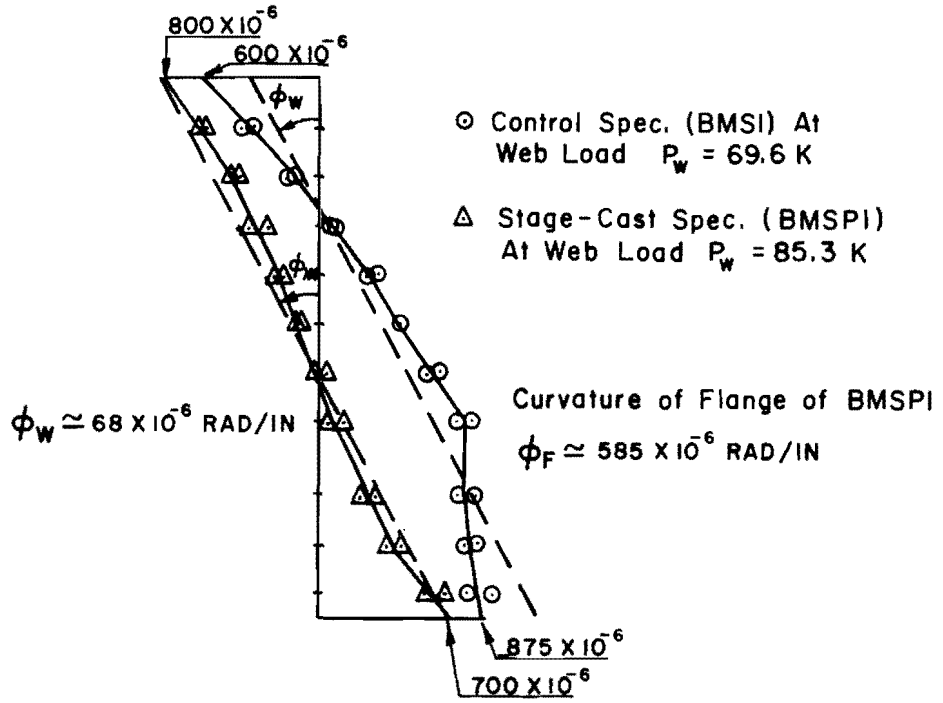

(a) At ϕ_w (Curvature Due to Web Load) $\simeq 68 \times 10^{-6}$ Rad/In

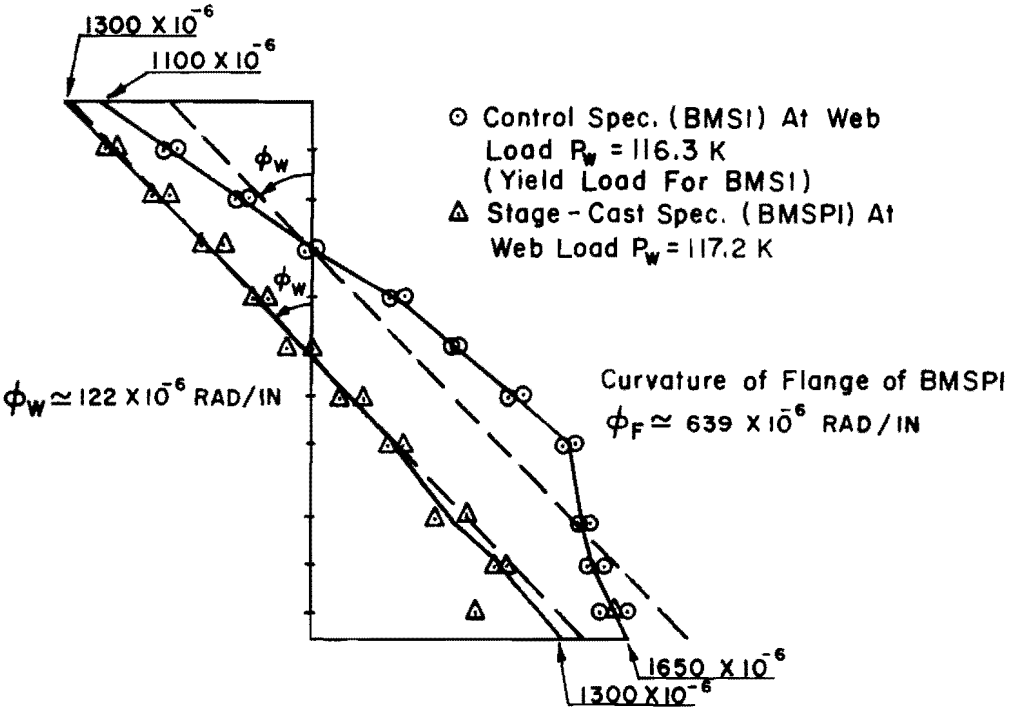

(b) At ϕ_w (Curvature Due to Web Load) $\simeq 122 \times 10^{-6}$ Rad/In

Fig. 3.7 Comparison of strain profiles of specimens BMS1 and BMSP1

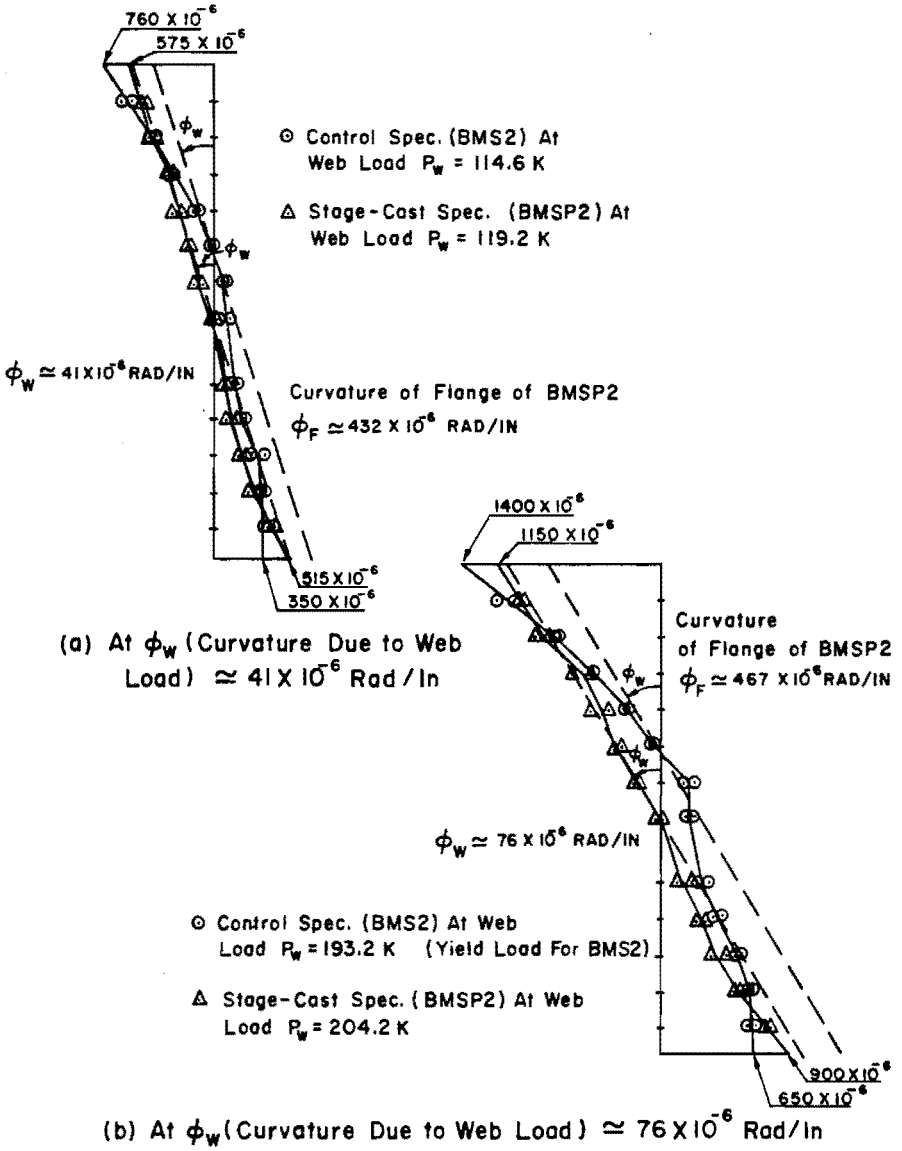

Fig. 3.8 Comparison of strain profiles of specimens BMS2 and BMSP2

at the same average change in live load curvature. Actually the changes in strain profile were remarkable similar for both the stage-cast and the control specimens in the load ranges illustrated. While approximately the same reserve compression stress capacity existed in both specimens, the larger tensile strains in the stage-cast specimen would permit steel to yield and appear to exhibit more ductile load resistance than that of the control specimen.

3.2 Creep Deflection of Preloaded Flange

Figure 3.9 shows the deflection-log time curves for 6 in. and 11 in. flanges, under a constant load that produced a 45 ksi stress in tensile reinforcement before the webs were cast. Vertical straight lines in Fig. 3.9 show instantaneous deflections due to load adjustments which are shown only where the adjustments were appreciable. An approximately equal slope of deflection-log time curves between all load adjustments indicates that the deflection-time relationship can be represented by an exponential curve as reported by Ferguson.[3]

Total creep deflection in seven days was found to be 14 percent of the instantaneous deflection for the 6 in. flange and 18 percent of that for the 11 in. flange, as shown in Table 3.1. The nominal compressive stress reached about 4200 psi in the 11 in. flange, but only 3500 psi in the 6 in. flange. Creep deflection in the 6 in. flange was 30 percent more than that in the 11 in. flange for a period of one week.

The average rate of creep, expressed as the amount of creep deflection per day, on the seventh day after loading dropped to 18 percent of the initial rate for the 6 in. flange and to 11.5 percent for the 11 in. flange.

Each stage-cast web was cast one to two weeks after flange loading, which is usually the period for which construction loads are applied on the flange in practice, regardless of the rate of creep deflection at the time of casting.

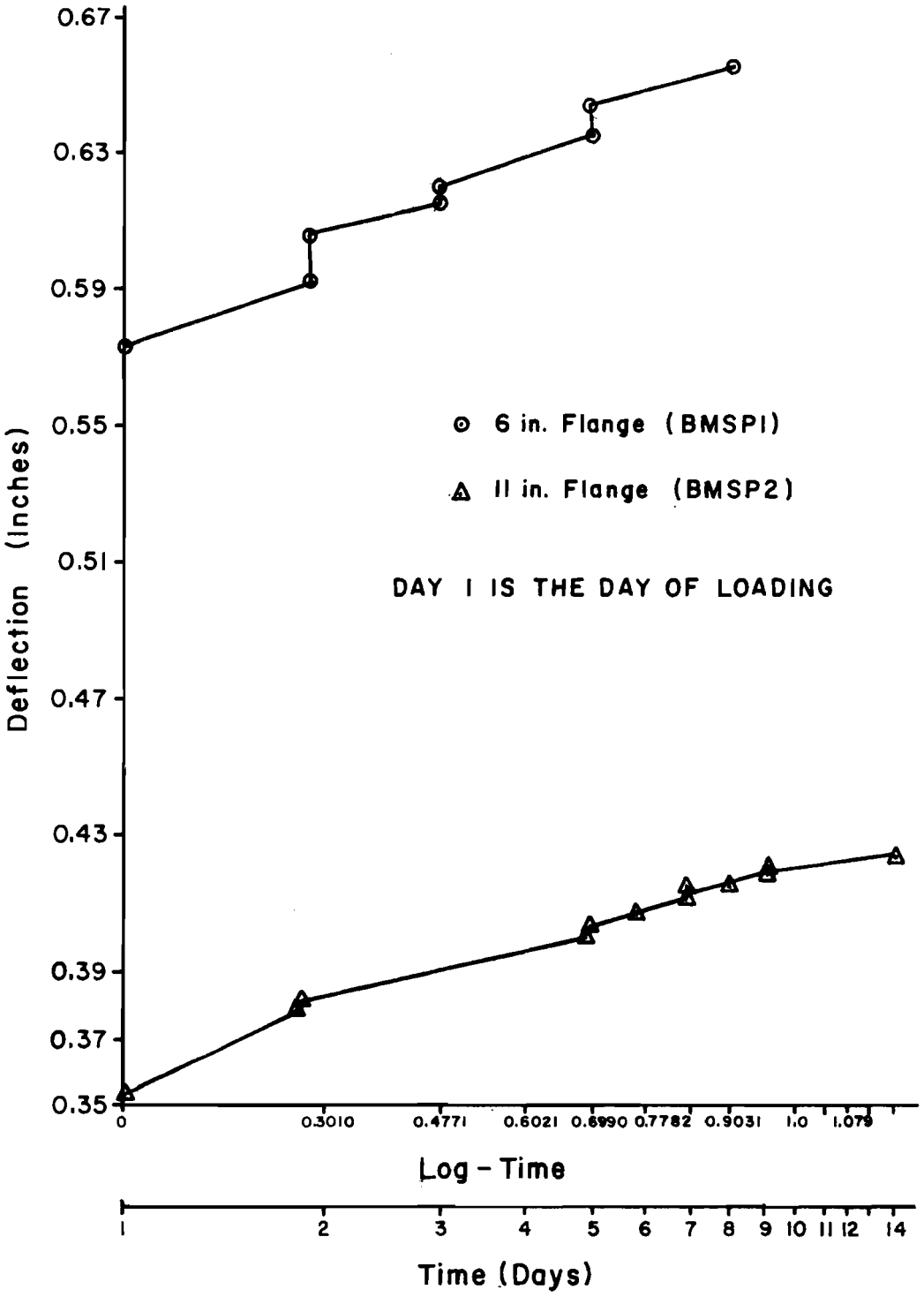

Fig. 3.9 Deflection-log time curves for flanges under constant load ($f_s \simeq 45$ ksi)

TABLE 3.1 CREEP DEFLECTIONS IN PRELOADED FLANGES AT 45 KSI STEEL STRESS

Flange of Specimen	t_f in.	b in.	d_f in.	p_f	p'_f	f'_c at the day of loading psi	Estimated top fiber conc. stress f_c psi	Approx. age at loading days	Total applied load P_f kips	Δ Instantaneous deflection at midspan in.	Additional creep deflection in seven days in.	Average rate of deflection on 1st day in./day	Average rate of deflection on 7th day in./day
BMSP1	6.175	22.163	4.938	0.017	0.004	5788	3528	39	16.0	0.574	0.081	0.0190	0.0034
BMSP2	11.084	21.950	9.703	0.019	0.002	5173	4231	120	72.0	0.353	0.063	0.0260	0.0030

3.3 Load-Deflection Relations

Deflection at midspan was measured by two dial gages. Load-deflection curves plotted in Figs. 3.10 and 3.11 show that the total midspan deflection of stage-cast specimens at ultimate was approximately twice as much as that of the control specimens and that the ultimate load of stage-cast specimens was slightly less than that for control specimens. It may also be interesting to observe that for the beams tested, approximately half of the total ultimate deflection in stage-cast specimens was due to the instantaneous and creep deflection of the flange caused by preloading of the flange.

3.4 Stiffness for Live Load

Throughout this report the term live load will be used to represent any load which was applied to a stage-cast beam after the stage-cast web had cured sufficiently to support the load in composite action with the precast flange. For control specimens the term live load will mean the total applied load minus the flange load of the corresponding stage-cast specimen.

Live load-deflection curves for the specimens are shown in Figs. 3.12 and 3.13. These curves display only those deflections which occurred after web loads were applied.

Stage-cast specimens appeared to be about two times as stiff as control specimens subjected to the same change in service live loads. The uncracked precompressed portion of flange resulted in a greater apparent moment of inertia and a greater stiffness for stage-cast specimens at service live loads. As the load increased the stiffness of stage-cast specimens reduced, due to the propagation of cracks into the precompressed zone of the flange. The stiffness of control specimens, however, remained almost constant over a wide range of live load as shown by live load-deflection curves (Figs. 3.12 and 3.13). Stage-cast specimens reached yield stress in tension reinforcement at live loads 27 to 40 percent lower than those resisted by control specimens before yielding took place. After yielding the stiffness of stage-cast

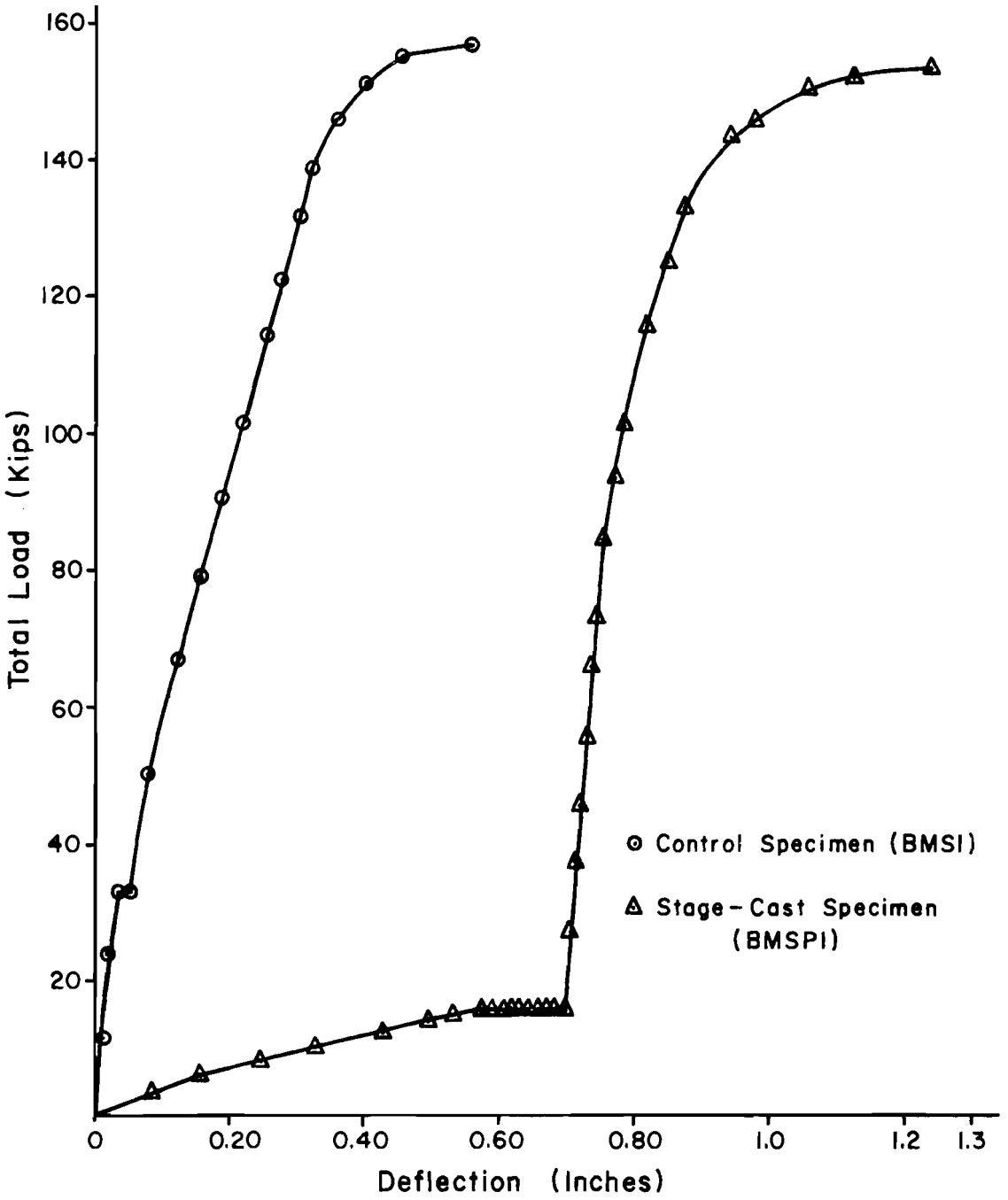

Fig. 3.10 Load-deflection curves for BMS1 and BMSP1

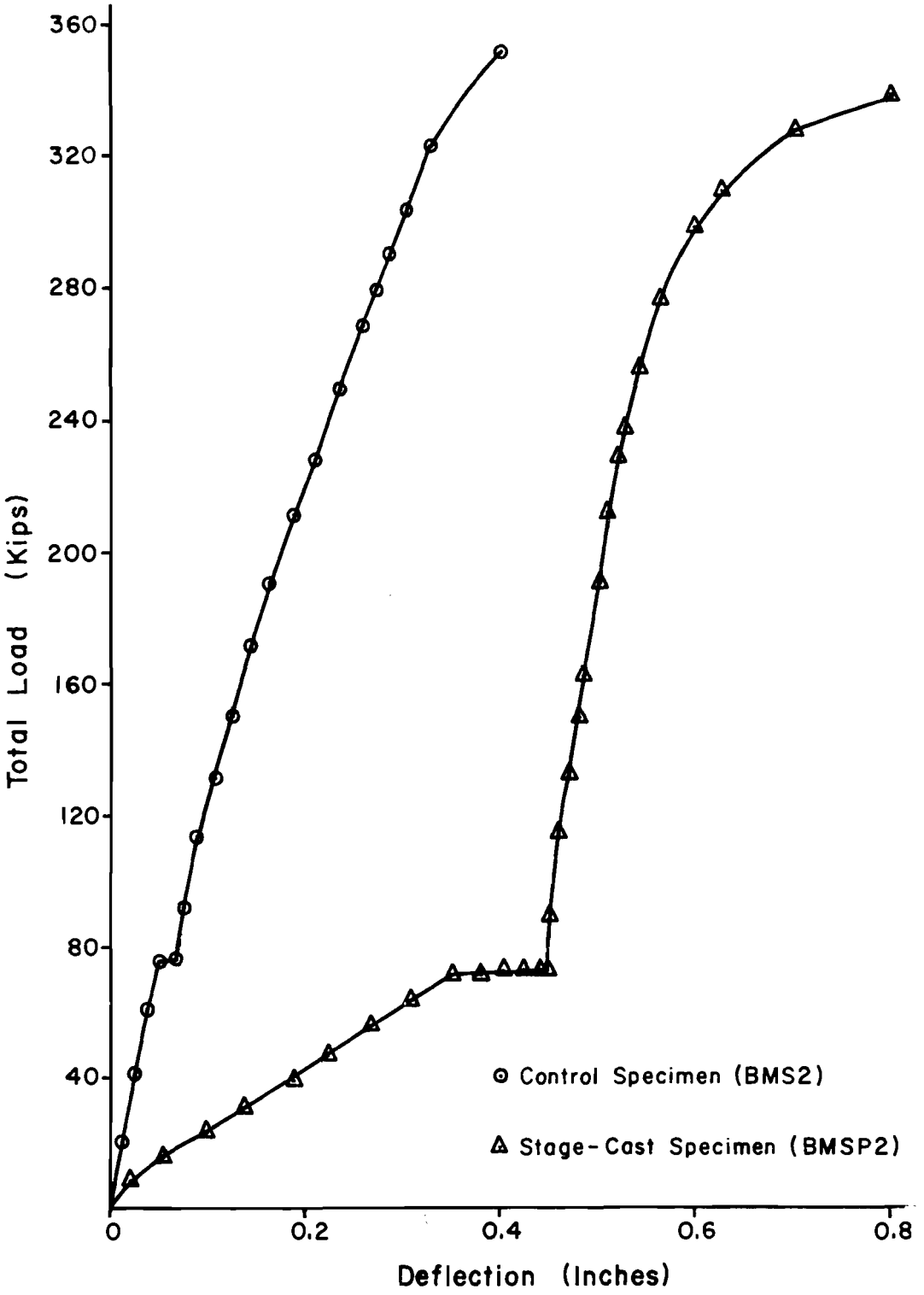

Fig. 3.11 Load-deflection curves for BMS2 and BMSP2

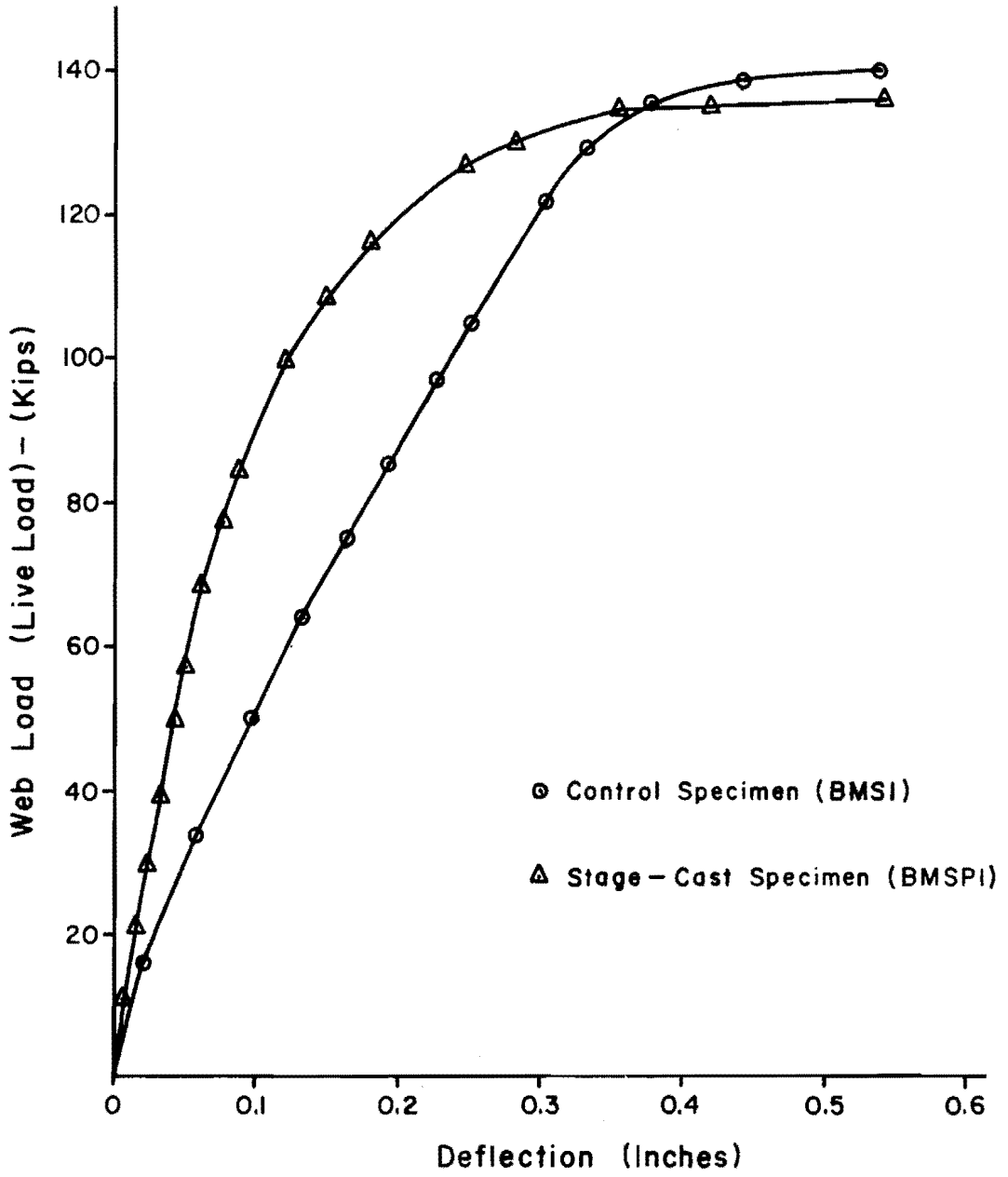

Fig. 3.12 Comparison of live load-deflection curves for BMS1 and BMSP1

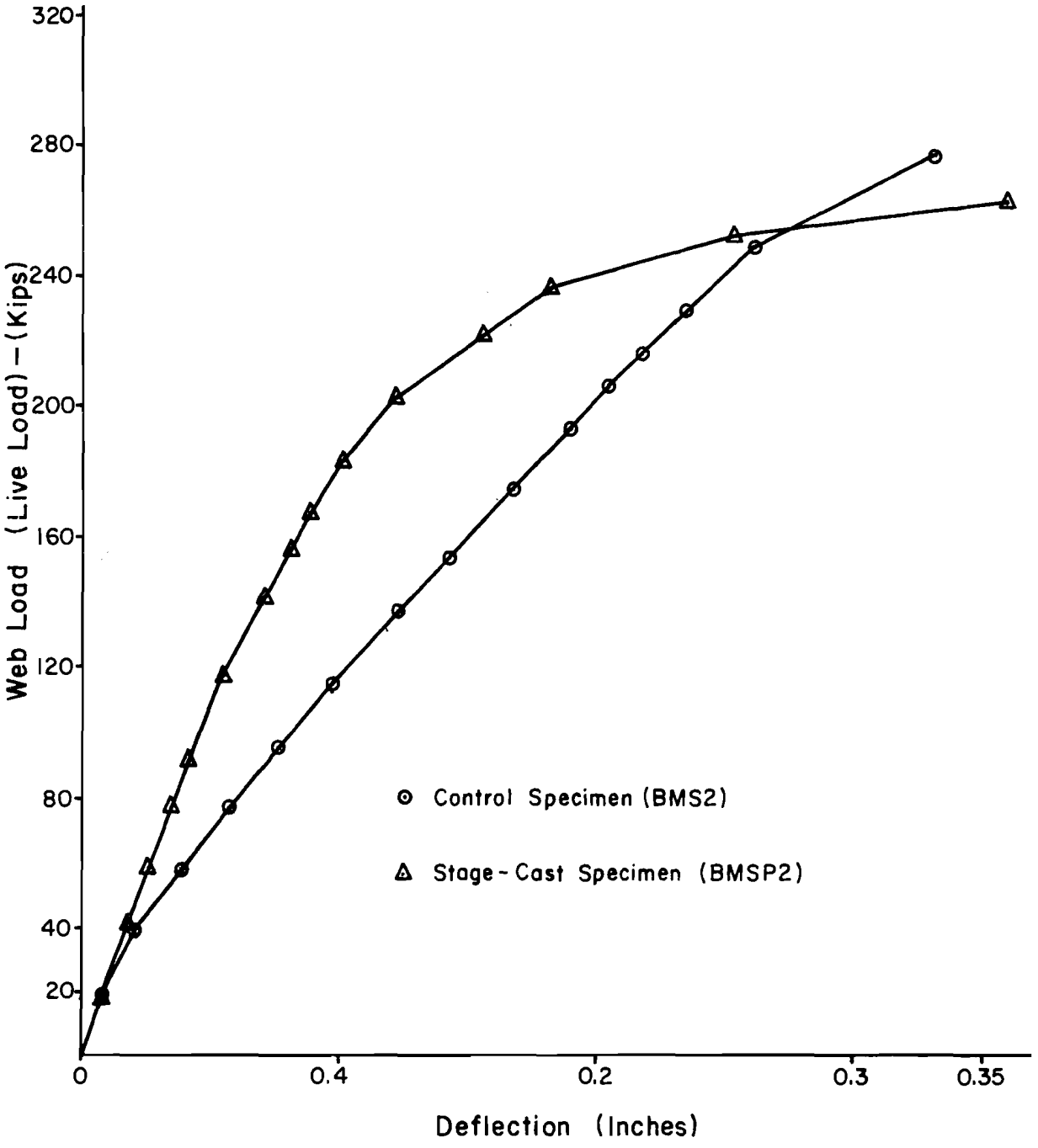

Fig. 3.13 Comparison of live load-deflection curves for BMS2 and BMSP2

specimens decreased at a greater rate. The stiffnesses of stage-cast and control specimens were found to be equal at the load at which the tension steel of the control specimens reached yield stress. Beyond this load, stage-cast specimens were less stiff than the control specimens.

The total live load deflection prior to collapse was virtually the same for both the stage-cast and the control specimens.

Stage-cast specimens possessed more apparent ductility than the control specimens because yielding of steel of stage-cast specimens took place at a lower live load and live load deflection, but flexural failure of stage-cast specimens took place virtually at the same ultimate load and deflection at which the control specimens failed.

3.4.1 Effect of Flange Depth-Total Depth (d_f/d) Ratio. Values of stiffness ratio presented in Table 3.2 show a close agreement between the stiffness ratios of BMSP1 and BMS1 ($d_f/d = 0.236$) and those of BMSP2 and BMS2 ($d_f/d = 0.387$), except at the zero live load. Flange depth-total depth ratio, therefore, does not seem to affect the live load stiffness of stage-cast beams as compared to similar monolithic beams.

3.5 Cracking

3.5.1 Crack Width. Crack width was measured at eight stations located on comparatively wide cracks so that the maximum crack width could be measured. The size of other wide cracks was also checked frequently to make sure that new cracks were not wider than the ones being measured. When new cracks became the largest cracks, another location for crack size measurement was established at the widest observed crack.

Figures 3.14 and 3.15 show the maximum crack widths at various load stages. Despite the care taken to locate the crack of maximum size, the widest crack in BMSP2 near ultimate load went unnoticed.

TABLE 3.2 COMPARATIVE STIFFNESSES FOR LIVE LOAD

Specimens	Desired depth d in.	p	d_f/d	Live load (web load) at (kips)				Stiffness ratio = (live load stiffness of stage-cast specimen) ÷ (live load stiffness of control specimen) at load P =				
				Service load*	Yielding of stage-cast specimen	Yielding of control specimen	Ultimate	Dead load only (zero LL)	Service load*	Yield load of stage-cast specimen	Yield load of control specimen	Ultimate load
BMS1 and BMSP1	20.75	0.0135	0.236	44.0	85.3	116.3	137.1	3.4	2.3	1.5	0.95	0.35
BMS2 and BMSP2	25.625	0.0218	0.387	76.4	119.2	196.7	265.4	1.0	1.9	1.9	1.2	0.23

*Service load, based on AASHTO load factors of 1.30 for dead load and 2.17 for live load plus impact, was determined by rectangular stress block method.

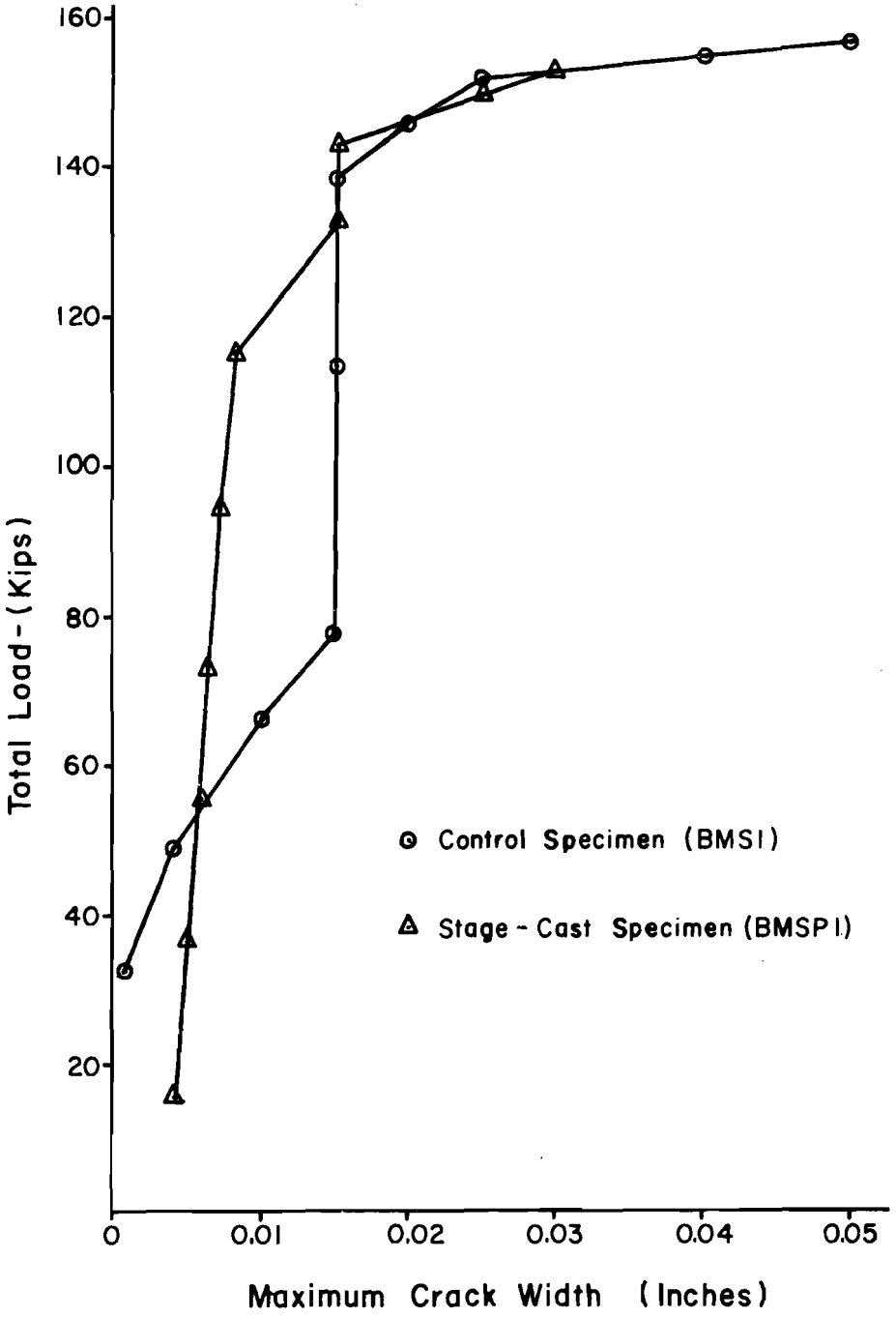

Fig. 3.14 Load-crack size relation for BMS1 and BMSP1

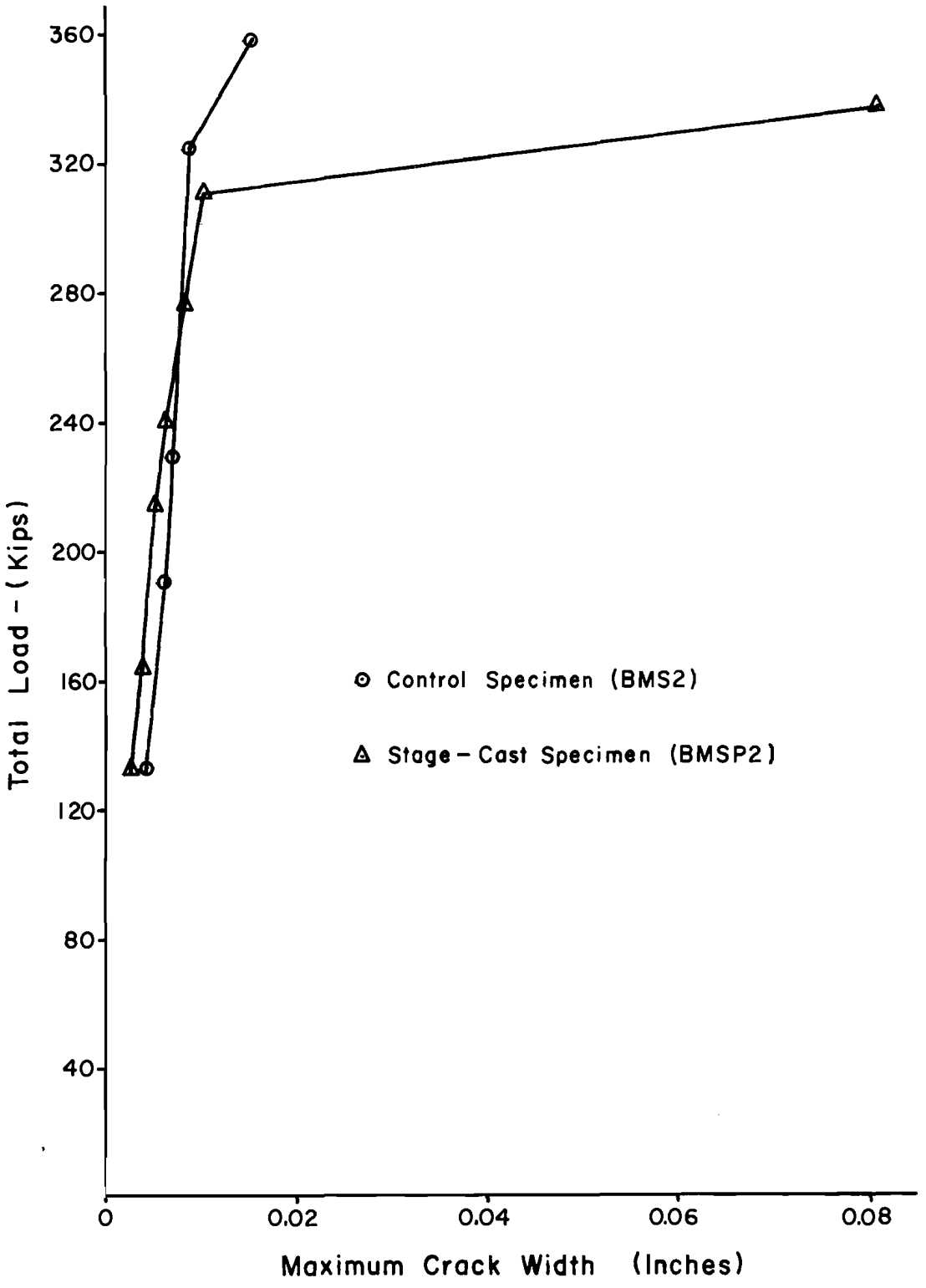

Fig. 3.15 Load-crack size relation for BMS2 and BMSP2

This crack was located right below the flange load point and it widened rapidly near the final load stages to a width of 0.08 in. at ultimate.

3.5.1.1 Effect of Stage-casting. Control specimens cracked at full flange load (cracks were visible one day after the loading). The crack width at this stage was less than 0.001 in., as shown in Table 3.3. The least count of the comparator used for crack size measurement was 0.001 in., hence the actual width of these cracks could not be recorded. Maximum crack width in BMSP1 was 0.004 in., and in BMSP2 was 0.001 in. at full flange load, just before loads were applied on the web--flange loads equivalent to 45 ksi of stress in tension steel were maintained on the flange of BMSP1 for seven days before casting of the web and for an additional period of 38 days before the application of the web load; flange loads on BMSP2 were maintained for 13 days before and 27 days after the casting of the web. Due to wider cracks created by the flange load, maximum crack width in stage-cast specimens was greater in the usual range of everyday load. Wider cracks existed in BMSP1 and BMSP2 up to a live load equal to 86 percent and 50 percent of that at full service load, respectively (see Figs. 3.14 and 3.15). For higher loads, cracks in control specimens were wider until the yielding of steel of control specimens. After yielding, crack width was found to be greater in the control specimen of 22-in.-deep beam, but was found to be more in the stage-cast specimen of 27-in.-deep beam.

Even though comparatively wider cracks existed in stage-cast beams at service live loads, these cracks were small enough to be permitted according to the recommendations of CEB (European Committee on Concrete), shown in Table 3.4. A maximum crack width of 0.004 in. in BMSP1 at full flange load (i.e., at full dead load and no live load) seems to be permissible as the major portion of creep due to flange (or dead) load had already taken place in the flange and cracks were not expected to widen appreciably with the passage of time due to further creep under dead load. However, special protection against

TABLE 3.3 MAXIMUM MEASURED CRACK WIDTHS FOR SPECIMENS

Specimen	Desired depth d (in.)	Span-flange thick-ness ratio L/t_f	p	Total service load (from AASHTO load factors) (kips)	Yield load for stage-cast specimen (kips)	Yield load for control specimen (kips)	Ultimate load (kips)	Maximum measured crack width, at: Full DL (zero LL) (in.)	Service load (in.)	Yield load of stage-cast spec. (in.)	Yield load of control specimen (in.)	Ultimate load (in.)	Total load at which the maximum crack width is: 0.004" (kips)	0.008" (kips)	0.012" (kips)
BMS1	20.75	18.3	0.0135	60.0	101.3	132.3	156.2	<0.001	0.008	0.015	0.015	0.050	49.0	60.0	71.0
BMSP1	20.75	18.3	0.0135	60.0	101.3	132.3	153.1	0.004	0.006	0.0075	0.015	0.030	16.0	116.0	126.0
BMS2	25.625	10.0	0.0218	148.4	191.2	268.7	346.0	<0.001	0.005	0.006	0.008	0.015	135.0	268.7	341.0
BMSP2	25.625	10.0	0.0218	148.4	191.2	268.7	337.4	<0.001	0.003	0.005	0.008	0.080	164.0	268.7	312.0

TABLE 3.4 CEB RECOMMENDATIONS FOR DEFORMED BARS

	Members Exposed to Very Aggressive Condition	Ordinary Structural Members	
		Unprotected	Protected
Maximum crack width (w_{max}), in.	0.004	0.008	0.012

corrosion may be necessary if the structure is located in very aggressive atmospheric conditions for beams like BMSP1 with comparatively thin flanges (span-to-flange thickness ratio for BMSP1 = 18.3). Cracks less than 0.005 in. in width are usually considered to be invisible from a distance. For the specimens tested, crack size in similar stage-cast and control specimens was found to exceed 0.005 in. at approximately equal loads. Maximum crack width reached 0.008 in. in BMSP1 at a load of 116 kips and at a load of 60 kips (maximum service load) in BMS1. Both BMS2 and BMSP2 had 0.008 in. wide cracks at a load of 268.7 kips (yield load for BMS2). Load for a crack width of 0.012 in. was much higher for BMSP1 than that for BMS1. Loads for this crack size were close to ultimate load in the case of BMS2 and BMSP2.

It is interesting to note that crack width in a stage-cast beam at a certain load depends not only on the depth of the composite section but also on the depth of the flange. At low live loads maximum crack width depends on the span-flange thickness ratio, i.e., at low live loads specimens with thin flanges are expected to have wider cracks. The increase in crack width due to live loads depends more on the depth of the composite section than that of the flange. An increase in crack width due to live load is slower in stage-cast beams because live load moments are partially resisted by the increase in lever arm, while the increase in steel strain is comparatively small.

In short, the test results show that cracks large enough to be distinctly visible were produced in stage-cast and control specimens

approximately at the same load. Cracks wider than permissible limits for prevention of corrosion under ordinary conditions (Table 3.4) were produced in stage-cast specimens at loads equal to (if not greater than) that for similar control specimens. Under highly aggressive atmospheric conditions, stage-cast beams with thin flanges (high span-flange thickness ratio) may need special protection against corrosion.

3.5.1.2 Effect of Depth. Cracks widened more rapidly in the shallow beams BMS1 and BMSP1. A crack width of 0.008 in. (maximum permissible crack size under ordinary conditions) was observed in BMS1 at service load, and at 1.93 times the service load in BMSP1. The same crack width was observed in deeper beams BMS2 and BMSP2 only at yield load. Hence, maximum crack width at a certain load was found to depend upon the depth of section more than on the stage-casting sequence. The width of cracks in stage-cast beams at low live loads was found to depend on the depth of the flange and at high loads on the depth of the composite T-section, as already mentioned under the preceding subsection.

Thus, crack widths remained less than 0.01 in. for all beams until loads reached 80 percent of ultimate values. Cracks remained smaller in stage-cast specimens than in control specimens at the same stage of loading. Even with a scale factor of 3, it can be concluded that cracks remained within acceptably small limits at service live load levels for all four specimens in this study.

3.5.2 Extent of Cracking. Cracking patterns and the extent of cracking as loading progressed are shown in Figs. 3.16 through 3.19. The numbers along each crack indicate the load sequence at which the extent of cracking was marked. A comparatively large number of flexural cracks were observed in the flanges of stage-cast specimens, considerably more than in the flanges of the control specimens.

Table 3.5 shows typical crack spacings and maximum heights to which the cracks extended at different loads.

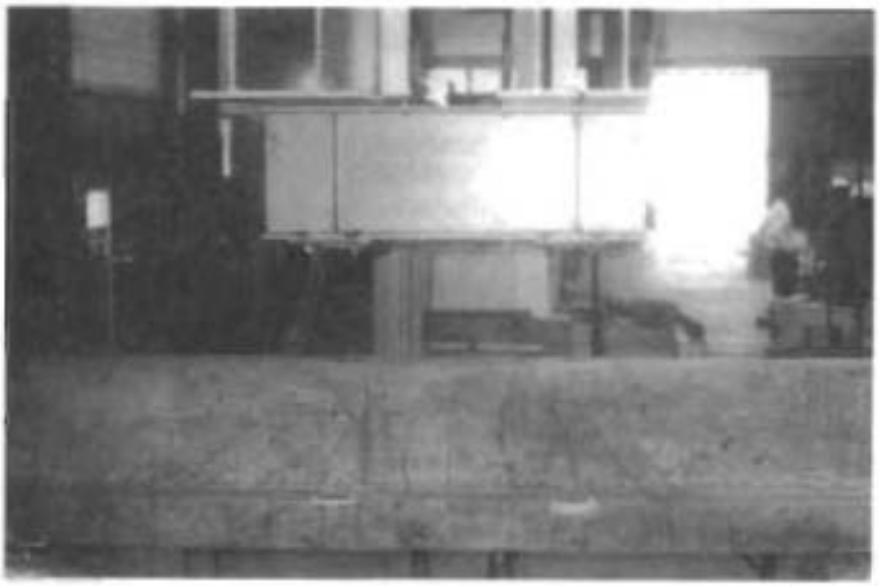

Fig. 3.16 Cracking pattern and extent of cracking in specimen BMS1

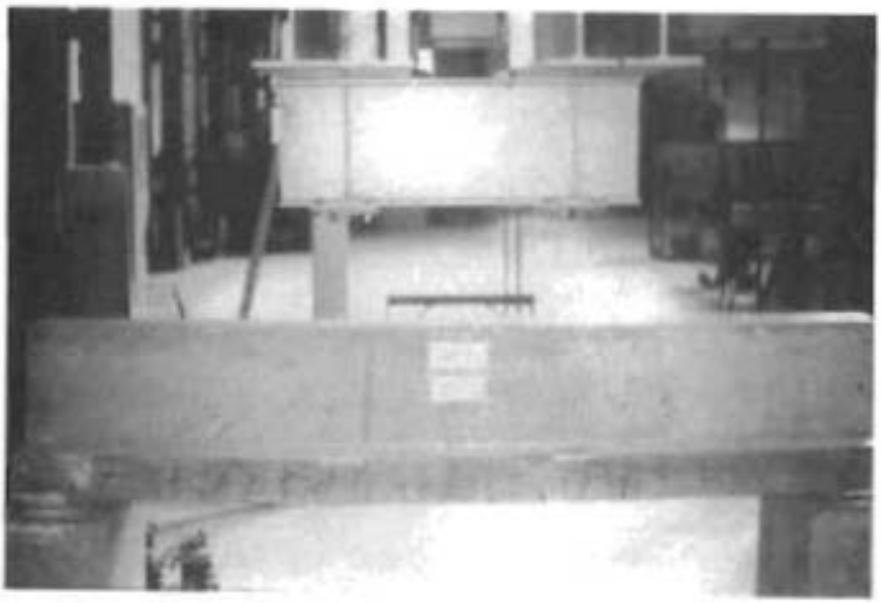

Fig. 3.17 Cracking pattern and extent of cracking in specimen BMSP1

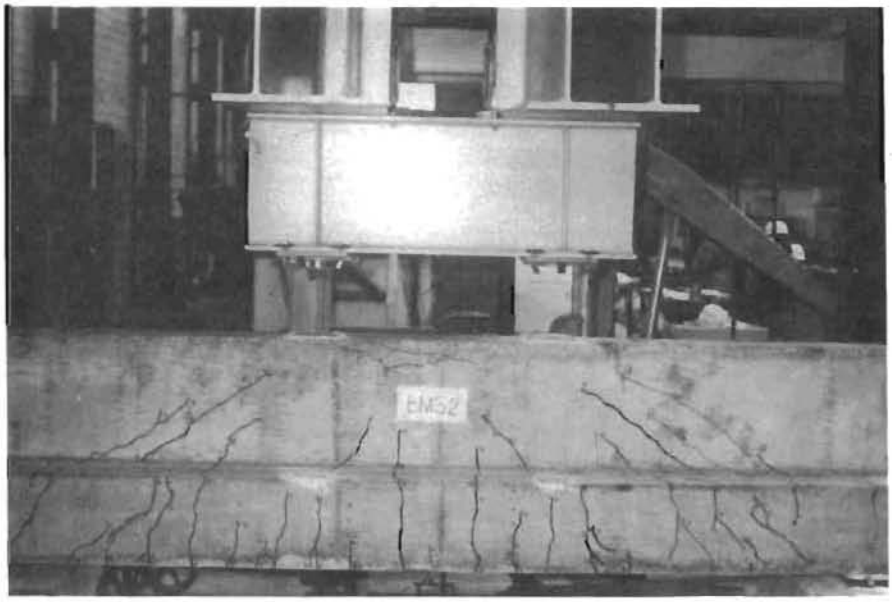

Fig. 3.18 Cracking pattern and extent of cracking in specimen BMS2

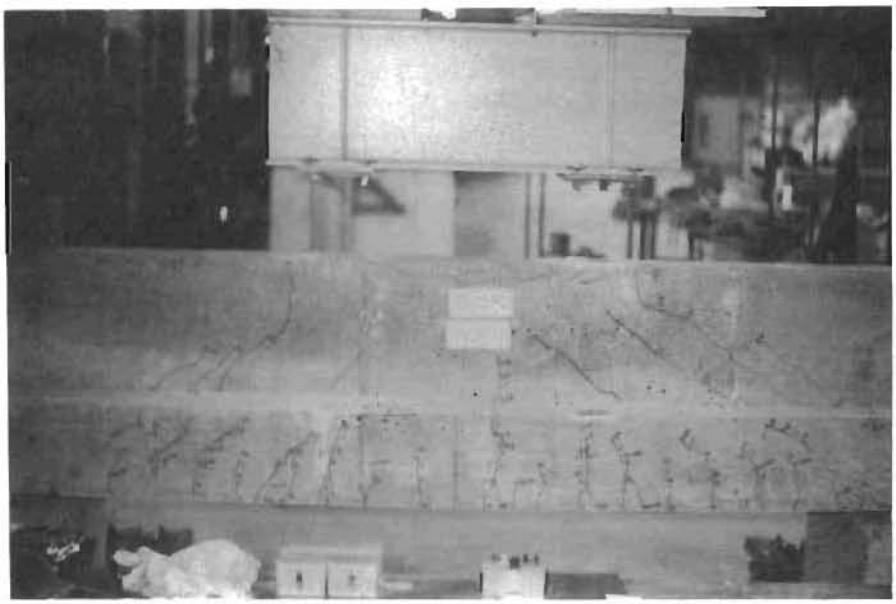

Fig. 3.19 Cracking pattern and extent of cracking in specimen BMSP2

TABLE 3.5 TYPICAL CRACK SPACING AND EXTENT OF CRACKING

Specimen	Typical crack spacing					Maximum height to which the cracks extended (measured vertically from bottom fiber					Total load at which flange top cracked (kips)
	at full DL (zero LL) (in.)	at service load (in.)	at yield load of stage-cast specimen (in.)	at yield load of control specimen (in.)	at ultimate (in.)	at full DL (zero LL) (in.)	at service load (in.)	at yield load of stage-cast specimen (in.)	at yield load of control specimen (in.)	at ultimate (in.)	
BMS1	10.0	6.0	6.0	6.0	6.0	5.0	11.6	17.3	18.0	18.3	49.8
BMSP1	3.0	3.0	3.0	3.0	3.0	3.5	4.25	6" in web* 4.25	12.7	17.7	116.1
BMS2	2 cracks only; below load points	5.0	5.0	5.0	5.0	5.0	16.35	16.6	21.5	24.2	133.2
BMSP2	4 to 5	4 to 5	4 to 5	3 to 5	3 to 5	6.75	7.25	7.5	10.5" in web* 9.5	22.5	337.4

*Measured from top of flange

Typical crack spacing was about 3 in. in BMSP1 and 6 in. in BMS1. Crack spacing was between 4 and 5 in. (5 in. typically) in BMSP2 and 5 in. in BMS2. Cracks at service load extended up to a height greater than 0.5d (up to 52 to 65 percent of d) from the bottom fiber in control specimens, but only up to 21 to 29 percent of d in stage-cast specimens. No crack extended into the web of stage-cast specimens at service load.

3.6 Strength

3.6.1 Ultimate Strength. The specimens were loaded until crushing of concrete was observed near the top of the web near mid-span. Crushing of concrete took place gradually as the load was applied, at a top fiber strain of 0.0031 to 0.0046. The crushing zone was found to be 2 to 3 in. deep and it extended 10 to 15 in. along the top surface of the beams.

Ultimate load capacities of the test specimens and a value for ultimate moment adjusted to a reference concrete strength f'_c = 4000 psi, specimen width b_w = 8.0 in., and specimen depth d = 20.11 in. for BMS1 and BMSP1, or 24.86 in. for BMS2 and BMSP2, are shown in Table 3.6. The corrected value of ultimate moment was obtained by multiplying the actual ultimate moment by a correction factor of $[20.11 - f'_c b_w a/(4000 \times 8.0 \times 2)]/(d - a/2)$ for BMS1 and BMSP1 and $[24.86 - f'_c b_w a/(4000 \times 8.0 \times 2)]/(d - a/2)$ for BMS2 and BMSP2. In each expression, "a" represents the height of rectangular stress block at ultimate. The correction factor was obtained using the rectangular stress block to represent concrete. It was assumed that small changes in steel strain at ultimate did not change the steel stress appreciably.

Corrected ultimate moment capacity for stage-cast specimens was found to be about 5 percent less than that for control specimens for beams of both sizes, as shown in Table 3.6.

Flexural cracks were observed at ultimate load to extend up to the top of the flange of stage-cast specimens, indicating that

TABLE 3.6 ULTIMATE MOMENT OF SPECIMENS

Specimen	b_w (in.)	d (in.)	d_f/d	f'_c (psi)	p_w	Ultimate moment from test (k-in.)	Ultimate moment corrected to f'_c=4000 psi, b_w=8.0 in., and d=20.11 in. or 24.86 in.*	(Corr. Ult. Moment of Stage-cast) ÷ (Corr. Ult. moment of control spec.) x 100
BMS1	8.25	20.270	0.236	4846	0.0135	3159	3053	95.3%
BMSP1	9.05	21.208	0.236	4004	0.0135	3099	2908	
BMS2	8.313	25.144	0.387	5208	0.0218	7092	6547	94.9%
BMSP2	7.875	25.503	0.387	5539	0.0218	6798	6215	

*d = 20.11 in. for BMS1 and BMSP1 and d = 24.86 in. for BMS2 and SMSP2.

all of the precompression due to preloading of the flange was lost before ultimate load was applied. Therefore, the internal couple resisting the ultimate moment was provided by compression in web concrete and tension in flange steel, as in the case of control specimens. Thus, the behavior of stage-cast specimens at ultimate was found to be similar to that of control specimens. However, it is possible to have stage-cast inverted T-beams with flange thickness-to-depth ratios large enough to retain some precompression in the flange even at ultimate. In that case, the ultimate moment capacity of stage-cast beams may be considerably less than that of similar monolithic beams. Hence, the ultimate strength of a stage-cast inverted T-beam can be considered as equal to that of a monolithic beam of the same size and reinforcement unless the flange depth to total beam depth ratio exceeds 0.4 ($d_f/d = 0.4$ for BMS2 and BMSP2).

3.6.2 Yield Moment Capacity. Measured yield moment capacities of the specimens are shown in Table 3.7. The yield moment capacities shown in the table may not be precisely accurate as those values were taken equal to the applied moment at the load stage immediately following the yielding of steel. Yield moment capacity of stage-cast specimens could not be converted easily and accurately to an adjusted capacity for the reference concrete strength f'_c = 4000 psi and the nominal specimen dimensions, because a part of the total flexural compression was present in the flange also. Hence, the yield moment capacity of control specimens was adjusted to match the concrete strength and the nominal size of corresponding stage-cast specimens. The corrected yield moment for control specimens shown in Table 3.7 was obtained by multiplying the actual yield moment of control specimens by a factor of $[d_s - f'_c b_w a/(2f'_{cs} b_{ws})]/(d - a/2)$, in which the subscript "s" indicates that the related quantity pertains to the corresponding stage-cast beam. The correction factor was derived using the rectangular stress block to represent concrete at yield load.

TABLE 3.7 YIELD MOMENT CAPACITY OF SPECIMENS

Specimen	b_w (in.)	d (in.)	d_f/d	f'_c psi	p_w	Yield moment from test (k-in.)	Yield moment of control specimens corrected to f'_c, b_w and d of corresponding stage-cast specimen (k-in.)	(Yield moment of stage-cast) + (Corr. yield moment of control specimen) x 100
BMS1	8.25	20.270	0.236	4846	0.0135	2681	2784	74.1%
BMSP1	9.05	21.208	0.236	4004	0.0135	2063		
BMS2	8.313	25.144	0.387	5208	0.0218	5424	5521	70.2%
BMSP2	7.875	25.503	0.387	5539	0.0218	3873		

Yield moment capacity of stage-cast specimens BMSP1 and BMSP2 was found to be 26 percent and 30 percent less than that of the corresponding control specimens BMS1 and BMS2. The difference between the yield moment capacities of stage-cast specimens and corresponding control specimens increased slightly with the increase in d_f/d ratio (flange depth to composite section depth ratio), but this increase (in difference between yield moments) was less than 4 percent for a 64 percent increase in d_f/d ratio. Hence, according to the test results, the yield moment for stage-cast beams (with d_f/d ratio between 0.2 and 0.4) does not depend on d_f/d ratio and may be about 30 percent less than that of similar monolithic beams.

A review of the flexural behavior of stage-cast specimens at a load equal to the yield load of similar control specimens may be interesting since most of the stage-cast beams are designed by neglecting the stresses and strains caused by the preloading of the flange, i.e., by assuming the stage-cast beam to be monolithically cast. As mentioned in Sec. 3.4 and 3.6.1, stage-cast specimens were found to be stiffer than the control specimens at all loads less than the yield load of the control specimens. Live load deflection of stage-cast specimens at ultimate load was virtually equal to that of the control specimens; live load deflection of stage-cast specimens was less than that of control specimens at all other loads. The ultimate strength of stage-cast specimens was the same as that of the control specimens. The ductility of stage-cast specimens was more than that of control specimens (see Sec. 3.7 also). Hence, stage-cast beams designed by the common procedure which neglects the effects of preloading of flange, are expected to possess sufficient strength and ductility and better serviceability than similar monolithically cast beams.

3.7 Ductility

A ductility factor of a structural member can be defined as the ratio of deflection at ultimate to the deflection at yielding of

the member (Δ_u/Δ_y). For the sake of comparison, ductility factors for stage-cast and control specimens, shown in Table 3.8, were computed using the deflections caused only by loads added after the web was cast rather the total load with corresponding deflections. Table 3.8 shows two values of a ductility factor for stage-cast beams--the actual value and the nominal value. The nominal value represents the expected ductility factor of a stage-cast beam designed by the commonly used design procedure which neglects all stresses and strains caused by the preloading of the flange. The nominal ductility factor is the ratio of the live load deflection at ultimate to the live load deflection at a load equal to the yield load of the corresponding control specimen.

The actual ductility factor of BMSP1 was 3.0 times that of BMS1 and the actual ductility factor of BMSP2 was 3.8 times that of BMS2.

The nominal ductility factors of the stage-cast specimens BMSP1 and BMSP2 were respectively 1.5 and 1.7 times those of the control specimens BMS1 and BMS2.

The above results indicate that stage-cast beams are expected to respond with considerably more apparent ductility than monolithically cast beams of the same size and reinforcement when each is subjected to superimposed live load after dead loads are applied.

TABLE 3.8 DUCTILITY FACTORS FOR SPECIMENS

Specimen	b_w (in.)	d (in.)	p	Deflections at midspan caused by web loads: at yield Δ_y (in.)	Deflections at midspan caused by web loads: at load equal to yield load of sim. control specimen Δ'_y (in.)	Deflections at midspan caused by web loads: at ultimate Δ_u (in.)	Ductility factor: Actual $= \Delta_u/\Delta_y$	Ductility factor: Nominal* $= \Delta_u/\Delta_y'$
BMS1	8.25	20.270	0.0135	0.2510	0.2510	0.5100	2.03	2.03
BMSP1	9.05	21.208	0.0135	0.0880	0.1800	0.5355	6.09	2.98
BMS2	8.313	25.144	0.0218	0.1895	0.1895	0.3325	1.75	1.75
BMSP2	7.875	25.503	0.0218	0.0547	0.1212	0.3597	6.58	2.97

*Ductility factor of stage-cast specimens, if strains caused by preloading of flange are neglected.

CHAPTER 4

STRENGTH ANALYSIS OF STAGE-CAST BEAMS

In this chapter results obtained by theoretical analyses are compared to the test results.

4.1 Ultimate Strength

Computations for ultimate strength of stage-cast beam BMSP2 are shown in Appendix A-3. Similar computations were made for BMSP1. It is interesting to note from the ultimate load computations that similar results would be obtained by analyzing BMSP2 (or BMSP1) as a monolithic beam, since no compression existed in the flange at ultimate load. Extreme fiber strain in concrete at ultimate was taken as 0.003 and the stress in steel was assumed to be equal to the yield stress of the steel, as recommended in Sec. 10.2.3 of the ACI Code (318-71).[1] The ultimate strength was computed both with the use of a rectangular stress block for concrete and by assuming a parabolic stress distribution in concrete.

4.1.1 Rectangular Stress Block Method. The ultimate strength of stage-cast specimens as predicted on the basis of a rectangular stress block to represent concrete stress were about 13 percent less than those found by test, as shown in Table 4.1. The details of ultimate strength computations for BMSP2 are shown in Appendix A-3.1. The ultimate moments of control specimens (Table 4.1) determined by a similar analysis were 17 to 18 percent less than the actual measured moments. A larger difference between the actual and the predicted ultimate moments for the control specimens was due to the fact that the control specimens were capable of supporting a load 5 percent greater than that supported by the stage-cast specimens at failure.

TABLE 4.1 ULTIMATE STRENGTH OF BEAMS DETERMINED BY DIFFERENT METHODS AS COMPARED WITH TEST RESULTS

Specimen	d_f/d	p	Ultimate Moment as determined by:			Ult. moment predicted by theory / Ult. moment found by test	
			Test (k-in.)	Rectangular stress block (k-in.)	Assuming stress distribution in concrete to be parabolic (k-in.)	Rectangular stress block method	Parabolic stress distribution in concrete
BMS1	0.236	0.0135	3159	2634	2638	0.834	0.835
BMSP1	0.236	0.0135	3099	2710	2721	0.874	0.878
BMS2	0.387	0.0218	7092	5835	5896	0.823	0.831
BMSP2	0.387	0.0218	6797	5926	5967	0.872	0.878

The predicted ultimate moments for similar stage-cast and control specimens differed by less then 3 percent. This difference was due to the tolerance in specimen dimensions and concrete strength.

4.1.2 Parabolic Stress Distribution in Concrete. Hognestad[18] suggested the following parabolic stress distribution function for concrete:

$$f_c = f_c'' [(2\epsilon/\epsilon_o) - (\epsilon/\epsilon_o)^2]$$

where ϵ is the compressive strain at a certain location, f_c is the stress in concrete corresponding to a compressive strain ϵ, f_c'' is the maximum stress in flexure (in this report f_c'' is assumed to be equal to f_c', the cylinder compressive strength), and ϵ_o is the strain corresponding to a concrete stress of f_c''.

Ultimate strength computations for BMSP2 using the above expression to represent the stress distribution in concrete are shown in Appendix A-3.2. The computed ultimate moment for similar stage-cast and control specimens differed by 1 to 3 percent, due to tolerance in specimen dimensions and concrete strength. The predicted ultimate strength was about 12 percent less than the actual for stage-cast specimens and 17 percent less than the actual for control specimens. A larger difference between the actual and predicted ultimate moments in the case of control specimens was due to the comparatively higher value of the actual ultimate moment.

4.1.3 Accuracy of the Analytic Methods. As mentioned earlier, the ultimate strength as predicted by the preceding analytical methods was 12 to 13 percent less than the actual in the case of stage-cast specimens, and 17 to 18 percent less than the actual in the case of control specimens. A comparatively low value of predicted ultimate strength was due primarily to the effects of neglecting strain hardening in steel. The estimated strain in steel at ultimate was 1.4 percent for BMSP1 and 0.9 percent for BMSP2. Strains as large as these are large enough to occur with strain hardening in steel. Both the above theoretical methods, therefore, seem to be quite accurate.

Inasmuch as the results obtained by the two methods were nearly the same, the rectangular stress block method is recommended because of its simplicity for representing concrete.

The predicted ultimate strengths of similar stage-cast and control specimens were equal, except for a less than 3 percent difference caused by the variations in the strength of concrete and the specimen dimensions. The ultimate strength of stage-cast beams, therefore, can be predicted by a comparatively simple analysis which neglects all strains (and stresses) caused by the preloading of the flange and utilizes a rectangular stress block to represent concrete stress, provided the flange thickness to overall depth ratio (t_f/h) for the beam is less than 0.41, the largest ratio observed in this study.

4.2 Strength at Yield

The test results indicate that considerable compressive strains (and stresses), caused by the flange preload, were present at the flange-web interface of the stage-cast specimens when yielding of the tension steel took place. The prediction of yield moment, the moment at which tension steel yields, for stage-cast beams, therefore, required two sets of calculations--the estimation of initial strains in the flange caused by the preloading, and the superposition of strain changes in the composite T-section caused by the web load. Initial strains in the flange have to be superimposed in order to determine the final strains (and internal forces) in the composite section. Details of yield moment computations for specimen BMSP2 are shown in Appendix A-4. Similar computations were made for specimen BMSP1.

Table 4.2 shows that compressive stresses as high as $0.63f'_c$ were present in the flange at yield load, while no compression existed in the flange at ultimate. This suggests that a comparatively simple analysis which neglects strains (and stresses) caused by the flange preload should not be used to calculate the yield moment of stage-cast

beams even though such an analysis is valid for predicting the ultimate moment as suggested in Sec. 4.1.3.

The maximum estimated concrete stress at yield load was $0.55f'_c$ in BMSP1 and $0.63f'_c$ in BMSP2, as shown in Table 4.2. Due to a comparatively low magnitude of stresses in concrete, the use of a rectangular stress block to represent concrete stress at yield load is not logical. A triangular stress distribution seems to be more reasonable in the above range of stresses.

4.2.1 Elastic Analysis. Yield moment of stage-cast beams as predicted by elastic analysis (assuming triangular stress distribution in concrete) was found to be 1 to 2 percent less than the actual yield moment of the specimens, as shown in Table 4.2.

Initial strains in the flange section caused by the preloading were computed as a part of the above yield moment calculations and these agreed fairly closely with those measured during the tests.

4.2.2 Parabolic Stress Distribution. Yield moment of stage-cast specimens, determined by using Hognestad's parabolic stress distribution equation for concrete, was found to be 1 to 2.5 percent less than the actual test value, as shown in Table 4.2.

Initial strains in the flange, computed as a part of the above yield moment calculations, agreed with the test values more closely than those calculated by using the elastic analysis.

4.2.3 Comparison of the Analytical Methods. The yield moment of a stage-cast beam can be predicted with sufficient accuracy by both analyses, either by assuming a parabolic stress distribution or a triangular stress distribution in concrete. Simplicity of calculations in elastic analysis (assuming triangular concrete stress distribution) makes it preferable over the one assuming parabolic stress distribution even though the latter predicts the strains more accurately. The additional "accuracy" is rarely appropriate, and a sense of such analytic precision could be misleading.

TABLE 4.2 YIELD STRENGTH OF STAGE-CAST SPECIMENS AS COMPUTED BY DIFFERENT METHODS

Specimen	d_f/d	p	Maximum Estimated Concrete Stress at Yield Load (psi) $\frac{\text{in Web}}{\text{in Flange}}$	Yield Moment* from Test (k-in.)	Yield Moment* of Corresponding Control Specimen from Test (k-in.)	Yield Moment Computed by Assuming		Yield Moment by Theory / Yield Moment by Test	
						Elastic Behavior (triangular stress dist. in concrete) (k-in.)	Parabolic stress distribution in concrete (k-in.)	For elastic analysis (triangular stress distribution)	For parabolic stress distribution
BMSP1	0.236	0.0135	$\frac{0.55f'_c}{0.31f'_c}$	2063	2681	2045	2050	0.991	0.994
BMSP2	0.387	0.0218	$\frac{0.42f'_c}{0.63f'_c}$	3873	5424	3806	3780	0.983	0.976

*Moment at the load stage following the yielding of tension steel.

CHAPTER 5

CONCLUSIONS

The main objective of the test program was to investigate whether stage-cast beams designed by the commonly employed design procedures are expected to have sufficient strength, ductility and live load stiffness, and whether the maximum crack size in such beams is expected to be within permissible limits.

Specimens tested were of two different sizes and different reinforcement--overall depth h = 22 in. and 27 in., overall flange tickness t_f = 6 in. and 11 in., and steel ratio $p_w = 0.47p_b$ and $0.76p_b$, respectively. Compressive strength of concrete (f'_c) varied from 4004 psi to 5788 psi.

The following conclusions are derived from the test results.

5.1 Extent and Size of Cracks

Maximum width of cracks in stage-cast specimens at low live loads depends more on the span-flange thickness ratio than on span-overall depth of composite section ratio. Cracks in stage-cast beams were, therefore, wider than those in the control specimens, at low live loads. The observed maximum crack size augmented by the appropriate scale factor indicated that crack size in a full scale stage-cast beam would be less than that permitted by CEB (European Committee on Concrete) standards for ordinary atmospheric conditions. In very aggressive atmospheric conditions, however, stage-cast beams with thin flanges may have corrosion problems. As a guide, an upper limit of 16 for span-flange thickness ratio is suggested by the 1971 ACI Code[1] for limiting the deflection of simply supported beams. It is considered to be adequate to limit the crack width also. However, more test

data are required to suggest a satisfactory upper limit for span-flange thickness ratio for stage-cast beams subjected to positive moment with the composite flange in tension.

Crack spacing was found to be fairly uniform throughout the span. Typical crack spacing was about 3 in. for the flange of stage-cast specimen BMSP1 and between 5 and 6 in. for the rest of the specimens. The total number of cracks in flanges was greater for stage-cast specimens but very few of the cracks in stage-cast beams extended into the web even at high loads.

5.2 Stiffness for Live Load

Live load stiffness for stage-cast specimens was more than that for control specimens, at all loads less than the yield load. At the service load the stage-cast specimens were approximately twice as stiff as the control specimens.

5.3 Ductility

Ductility factor (Δ_u/Δ_y) for stage-cast specimens was more than three times that for the control specimens. If deflection at a load equal to the yield load of the corresponding control specimen was used to compute the ductility factor, stage-cast specimens were found to be 1.5 to 1.7 times as ductile as the control specimens. Stage-cast beams, therefore, possess more ductility than similar monolithic beams.

5.4 Strength Analysis

5.4.1 Shape of Strain Profile. Strain profiles for the test specimens were found to be nearly linear in most cases. It is, therefore, reasonable to assume a straight line variation in strain along the depth of a flexural member, whether or not the flange is preloaded.

5.4.2 Ultimate Strength. Maximum strain in concrete at ultimate was found to be between 0.0031 and 0.0046. A value of 0.003

suggested by the 1971 ACI Code[1] as a lower limit to the ultimate concrete strain, therefore, seems to be reasonable.

Ultimate strength of stage-cast specimens can be computed by the method of analysis recommended by ACI Code (318-71). For stage-cast beams with flange thickness-overall depth (t_f/h) ratio not more than 0.41, the ultimate strength can be computed by assuming the beam to be monolithically cast, i.e., by neglecting the initial strains caused by the preloading of the flange.

5.4.3 Yield Strength. Yield strength of stage-cast specimens was found to be up to 30 percent less than that of the control specimens.

Analyses assuming compressive stress distribution in concrete as a parabola or triangle (elastic analysis) gave results within 2 percent of the test results. Elastic analysis seems to be reasonable at yield load as the strains at the top of the flange and the web were low enough to limit the compressive stress in concrete to $0.63f'_c$ ($0.55f'_c$ in most cases).

5.5 Behavior of Stage-cast Beams Designed as Monolithic Beams

Even though the yield strength of stage-cast specimens was found to be considerably less than that of control specimens, the test results suggest that stage-cast beams designed to carry a factored load equal to the yield load of a similar monolithic beam will perform equally well (if not better). The above statement is based on the following observations:

(1) Ultimate strength of stage-cast specimens was within 5 percent of that of control specimens.

(2) The ductility factor for stage-cast specimens was at least 1.5 times the ductility factor for control specimens.

(3) Live load stiffness of stage-cast specimens was equal to that of control specimens at yield load, and was more than the

stiffness of control specimens at service loads.

(4) Deflection due to live load was found to be less for stage-cast specimens at all loads less than 96 percent of the ultimate. At service loads, stage-cast specimens deflected 51 percent less than the control specimens.

(5) The width of cracks in stage-cast specimens was less than the permissible limits for ordinary atmospheric conditions. However, in very aggressive atmospheric conditions special protection against corrosion must be provided for stage-cast beams with thin flanges.

A P P E N D I X

A-1 DESIGN OF SPECIMENS BMS1 and BMSP1

1. Flange section:

b_f = 22.0 in.

t_f = 6.0 in.

d_f = 6 - 1 - 0.25 = 4.75 in. (for #4 bars)

f'_c = 4000 psi

f_y = 60 ksi

AASHTO load factor for dead load = 1.30

Steel stress at service dead load, $f_s \simeq 60/1.30 = 46.2$

Assume f_s = 45.0 ksi.

In order to have sufficient compression reserve at full flange load, take $p_f = 0.60 \times p_b = 0.171$

$A_{sf} = p_f b_f d_f$ = 1.79 sq. in.

Use 9 #4 bars (Area = 1.80 sq. in.)

Provide 2 - #4 bars near top of flange and near the top of web

2. Composite section (T-section):

b_w = 8.0 in.

d = 22 - (9 x 1.25 + 2 x 4.75)/11 = 20.11 in.

$p = A_s/b_w d = 0.137 < 0.75\, p_b$ OK

3. Estimate flange load:

Use Hognestad's[18] stress-distribution relation:

$f_c = f''_c[(2\epsilon/\epsilon_o) - (\epsilon/\epsilon_o)^2]$, take $f''_c = f'_c$

$E_c = 57000\sqrt{f'_c}$ = 3600 ksi

ϵ_o = 0.0019

Try c = 1.92 in.

ϵ_c = 0.00105

C_c = 76.3 k (by integration)

$\bar{x}$ = 1.24 in. (by integration)

C_s = 4.26 k

C = 80.6 k

T = 1.8 x 45 = 81.0 k $\simeq$ C

f_c = 3.20 ksi

M = 325.5 k-in.

P_f = 16.2 k (Equally distributed among 4 load points)

4. Ultimate load:

ϵ_{cu} = 0.003

Try c = 4.67 in.

ϵ_s = 0.0103 > ϵ_y

ϵ'_{sf} = 0.00808 > ϵ_y

T = 2.2 x 60 = 132 k

ϵ'_{sw} = 0.0022 > ϵ_y

C_s = 0.4 x 60 = 24 k

$C_c = 0.85f'_c ba$ = 108.0 k

C = 132k = T

M_u = 2411 k-in.

P_u = 120.6 k

P_w = 120.6 - 16.2 = 104.4 k (Equally distributed at two load points)

5. Shear design:

Design load for shear = $1.25P_u$ = 150.7 k

$1.25P_w$ = 130.3 k

$1.25P_f$ = 20.4 k

$v_u = V_u/bd$ = 454.1 psi

$v_c = 1.9\sqrt{f'_c} + 2500p_w(V_u d)/M_u$ = 134.3 psi

$3.5\sqrt{f'_c}$ = 221.4 > 134.3

$v_s = v_u - v_c$ = 319.8 psi

$s = A_v f_y/(b_w v_s)$ = 5.1 in., say 5.0 in.

Check stirrups as hangers:

$V_f = 2\sqrt{f'_c}\, b_f d_f + A_v d_f f_y/s$ = 25.8 k

$F = (d + b_w)A_v f_y/s$ = 76.0 k

$(F + V_f/2)$ = 88.9 k

Design load = 20.4/2 = 10.2k < 88.9k OK

Check for horizontal shear:

$V_h = 1.25P_w/2 = 65.2k$

$v_{dh} = V_u/b_v d = 0.405 \text{ ksi} > 0.350 \text{ ksi}$ Check shear friction

$A_{vf} = V_u/\bar{\phi} f_y\mu = 65.2/60 = 1.087 \text{ in.}^2$

No. of stirrups required = $1.087/0.22 = 4.94 < 24$ OK

Shear transfer at web-flange joint:

Assume elastic behavior

c.g. of composite (T-section) = 8.415 in. from bottom

$I = 10990 \text{ in.}^4$

$f_{\text{flange top}} = M/I_y = 0.531 \text{ ksi}$

$f_{\text{bottom}} = M/I_y = 1.85 \text{ ksi}$

$f_{\text{average}} = (f_{\text{flange top}} + f_{\text{bottom}})/2 = 1.1905 \text{ ksi}$

Design Shear = $1.25 f_{av} b_f t_f = 196.4k$

Shear resisted = (No. of Stirr.)$\mu A_v f_y = 316.8k > 196.4k$ OK

6. Bracket Design:

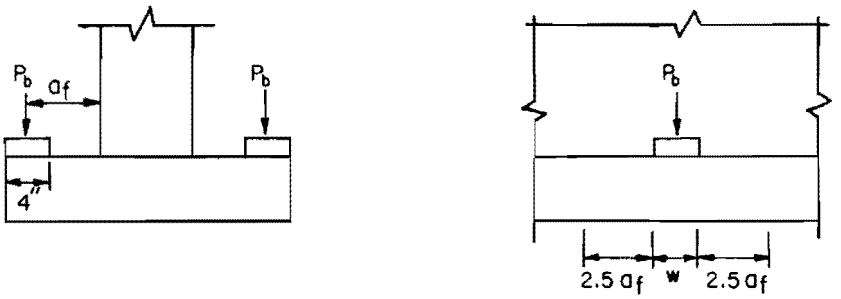

$a_f/d_f = 1.053 > 0.5$ Design for flexure

$P_b = 1.25p_f/4 = 5.1k$

$M_f = P_b a_f = 25.5 \text{ k-in.}$

$A_s = M_f/f_y j d_f = 0.112 \text{ in.}^2$

Min. steel from ACI Code

$A_s = 0.0018A_g = 0.0018t_f(5a_f + w) = 0.313 \text{ in.}^2$

Use #3 bars

$s = A_s/(2 \times 0.11) = 10.2 \text{ in.}$; say 10 in.

7. Shear reinforcement for flange:

t_f = 6 in. < 10 in. No shear reinforcement required

Use #3 U-bars at 10 in. spacing to support bracket reinforcement.

A-2 COMPUTED INITIAL STRAINS IN FLANGE OF SPECIMEN BMSP2

Estimated initial strains in concrete (at top fiber of flange) and steel due to flange load:

a. By elastic theory:

ϵ_{ci} = 0.0009663 ϵ_{si} = 0.001508

b. By parabolic stress distribution:

ϵ_{ci} = 0.0009911 ϵ_{si} = 0.001521

A-3 ULTIMATE STRENGTH OF SPECIMEN BMSP2

b_w = 7.875 in.
b = 21.875 in.
d_w = 16.563 in.
t_f = 11.078 in.; $d_u + t_f$ = 27.641
A'_s = 0.394 sq. in.
A_{sf} = 3.933 sq. in.
A'_{sf} = 0.394 sq. in.
d = 26.266 in.

d_f = 9.703 in.
f'_{cw} = 5539 psi
f'_{cf} = 5173 psi
f_y (#6 bars) = 60.7 ksi
f_y (#4 bars) = 65.5 ksi
E_s (#6 bars) = 29400 ksi
E_s (#4 bars) = 27400 ksi

A-3.1 Rectangular Stress Block

ϵ_{cu} = 0.003

Assume ϵ_{ci} = 0.0009911 (max. value, see A-2)

ϵ_{si} = 0.001521 (see A-2)

Try c = 8.357 in.

$\epsilon_{sw} = (d - c)0.003/c = 0.00643$

$\epsilon_s = \epsilon_{sw} + \epsilon_{si} = 0.00795 > \epsilon_y$

$\epsilon_{IF} = (d - d_f - c)0.003/c = 0.00295$

$\epsilon_{cf} = \epsilon_{ci} - \epsilon_{IF} = -0.00196$ (tensile)

$\epsilon'_{sf} = \epsilon_{cf} - (\epsilon_{cf} + \epsilon_s)d'_f/d_f = 0.00278 > \epsilon_y$

$T = A_s f_y + A'_{sf} f_y = 264.5k$

$C_{cw} = 0.85 f'_c ba = 238.6k$

$C_{cf} = 0 \qquad (\epsilon_{cf}$ in tensile)

$\epsilon'_{sw} = (c - d')0.003/c = 0.002321 < \epsilon_y$

$C_{sw} = A'_{sw} f_s = 25.1k$

$C = 263.7k \simeq T$

$M'_u = C_{cw}(d - a/2) + C_{sw}(d - d') - A'_{sf} f_y (d_f - d'_f) = 5926.$ k-in.

A-3.2 Parabolic Stress Distribution

$\epsilon_{cu} = 0.003$

$\epsilon_{ci} = 0.0009911 \quad ; \quad \epsilon_{si} = 0.001521$

$\epsilon_{ow} = 0.002229$

Try $c = 7.423$ in.

$C_{cw} = b f'_c (\alpha/\epsilon_o) c^2 [1 - (\alpha c/3\epsilon_o)] = 240.3k$

$\epsilon'_{sw} = (c - d')0.003/c = 0.002236 < \epsilon_y$

$C_{sw} = \epsilon'_{sw} E_s A'_{sw} = 24.1k$

$\epsilon_{sw} = (d - c)0.003/c = 0.00762$

$\epsilon_s = \epsilon_{sw} + \epsilon_{si} = 0.00914 > \epsilon_y$

$\epsilon_{IF} = (d - d_f - c)0.003/c = 0.00369$

$\epsilon_{cf} = \epsilon_{ci} - \epsilon_{IF} = -0.00270 \qquad$ (tensile)

$C_{cf} = 0$

$\epsilon'_{sf} = \epsilon_{cf} - (\epsilon_{cf} + \epsilon_s)d'_f/d = 0.00358 > \epsilon_y$

$C = C_{cw} + C_{sw} = 264.4k$

$T = A_s f_y + A'_{sf} f_y = 264.5k$

$\bar{x}_w = (8\epsilon_{ow} - 3\epsilon_{cu})c/(12\epsilon_{ow} - 4\epsilon_{cu}) = 4.445$ in.

$M'_u = C_{cw}(d - c + \bar{x}_w) + C_{sw}(d - d') - A'_{sf} f_y (d_f - d'_f) = 5967$ k-in.

A-4 YIELD STRENGTH OF SPECIMEN BMSP2

A-4.1 Parabolic Stress Distribution

$\epsilon_{ci} = 0.0009911 \quad ; \quad \epsilon_{si} = 0.001521$

$\epsilon_s = \epsilon_y = 0.002065$

$\epsilon_{sw} = \epsilon_s - \epsilon_{si} = 0.000544$

Try $c_w = 12.90$ in.

$\epsilon_{cw} = c_w\epsilon_{sw}/(d - c_w) = 0.000525$

$C_{cf} = b_w f'_{cw} c[1 - (\epsilon_{cw}/3\epsilon_o)]\epsilon_{cw}/\epsilon_o = 122.1k$

$\epsilon_{IF} = (d - d_f - c_w)\epsilon_{sw}/(d - c_w) = 0.0001443$

$\epsilon_{cf} = \epsilon_{ci} - \epsilon_{IF} = 0.0008468$

$c_f = \epsilon_{cf} d_f/(\epsilon_{cf} + \epsilon_s) = 2.822$ in.

$C_{cf} = b_f f'_{cf} c_f(1 - \epsilon_{cf}/3\epsilon_o)\epsilon_{cf}/\epsilon_o = 109.1k$

$\epsilon'_{sw} = (c_w - d')\epsilon_{sw}/(d - c_w) = 0.000448$

$C_{sw} = \epsilon'_{sw} E_s A'_{sw} = 4.8k$

$\epsilon'_{sf} = (c_f - d'_f)\epsilon_s/(d_f - c_f) = 0.000448$

$C_{sf} = 4.8k$

$C = C_{cw} + C_{cs} + C_{sw} + C_{sf} = 240.1k$

$T = A_s f_y = 238.7k \simeq C$

$\bar{x}_w = (8\epsilon_{ow} - 3\epsilon_{cw})c_w/(12\epsilon_{ow} - 4\epsilon_{cw}) = 8.508$ in.

$\bar{x}_f = 1.846$ in.

$M_y = C_{cw}(d - c_w + \bar{x}_w) + C_{cf}(d_f - c_f + \bar{x}_f) + C_{sw}(d - d') + C_{sf}(d_f - d'_f) = 3780$ k-in.

A-4.2 Elastic Analysis

$\epsilon_{ci} = 0.0009663$; $\epsilon_{si} = 0.001508$

$\epsilon_{sw} = \epsilon_y - \epsilon_{si} = 0.000557$

Try $c = 13.25$ in.

$\epsilon_{cw} = c_w\epsilon_{sw}/(d - c_w) = 0.000567$

$\epsilon'_{sw} = (c_w - d')\epsilon_{sw}/(d - c_w) = 0.000486$

$\epsilon_{IF} = (d - d_f - c_w)\epsilon_{sw}/(d - c_w) = 0.0001418$

$\epsilon_{cf} = \epsilon_{ci} - \epsilon_{IF} = 0.0008245$

$c_f = \epsilon_{cf} d_f/(\epsilon_{cf} + \epsilon_s) = 2.768$ in.

$C_{cw} = 0.5 f_{cw} c_w b_w = 125.5k$

$C_{sw} = f'_{sw} A'_{sw} = 5.2k$

$C_{cf} = 0.5 f_{cf} b_f c_f = 102.3k$

$\epsilon'_{sf} = (c_f - d'_f)\epsilon_s/(d_f - c_f) = 0.000429$

$C_{sf} = 4.6k$

$C = 237.6k$

$$T = A_s f_y = 238.7k \simeq C$$

$$M_y = C_{cw}(d - c_w/3) + C_{cf}(d_f - c_f/3) + C_{sw}(d - d') + C_{sf}(d_f - d'_f) = 3806 \text{ k - in.}$$

REFERENCES

1. American Concrete Institute, Building Code Requirements for Reinforced Concrete (ACI 318-71), Detroit, 1971.

2. American Concrete Institute, Commentary on Building Code Requirements for Reinforced Concrete (ACI 318-71), Detroit, 1971.

3. Ferguson, P. M., Reinforced Concrete Fundamentals, Third Edition, John Wiley & Sons, Inc., New York, 1973, pp. 12-13.

4. Timoshenko, S., and Goodier, J. N., Theory of Elasticity, Second Edition, McGraw-Hill Book Co., Inc., New York, 1951, pp. 166-171.

5. Department of Civil Engineering, The University of Missouri, "Structural and Economic Study of Precast Bridge Units: Instrumentation," Technical Report No. 1, Cooperative Research Project, Engineering Experiment Station, Columbia, 1957, pp. 6-16.

6. ACI-ASCE Committee 333, "Tentative Recommendations for Design of Composite Beams and Girders for Buildings," Journal of the American Concrete Institute, Vol. 32, No. 6, December 1960, pp. 609-628.

7. Badoux, J. C., and Hulsbos, C. L., "Horizontal Shear Connection in Composite Concrete Beams under Repeated Loads," Journal of the American Concrete Institute, Proc. V. 64, No. 12, December 1967, pp. 811-819.

8. Grossfield, B., and Brinstiel, C., "Tests of T-Beams with Precast Webs and Cast-in-place Flanges," Journal of the American Concrete Institute, Proc. V. 59, No. 6, June 1962, pp. 843-851.

9. Hanson, N. W., "Precast-Prestressed Concrete Bridges: (2) Horizontal Shear Connections," Journal of the PCA Research and Development Laboratories, Vol. 2, No. 2, May 1960, pp. 38-58.

10. Ozell, A. M., "Behavior of Single-span and Continuous Composite Prestressed Concrete Beams," Journal of the Prestressed Concrete Institute, Vol. 2, No. 1, June 1957, pp. 18-31.

11. Revesz, S., "Behavior of Composite T-Beams with Prestressed and Unprestressed Reinforcement," Journal of the American Concrete Institute, Vol. 24, No. 6, February 1953, Proc. V. 49, pp. 585-592.

12. Saemann, J. C., and Washa, G. W., "Horizontal Shear Connections between Precast Beams and Cast-in-Place Slabs," Journal of the American Concrete Institute, Proc. V. 61, No. 11, November 1964, pp. 1383-1409.

13. Broms, B. B., "Crack Width and Crack Spacing in Reinforced Concrete Members," Journal of the American Concrete Institute, Proc. V. 62, No. 10, October 1965, pp. 1237-1256.

14. Comité Européen du Béton, Bulletin d'Information No. 24, Paris, 1960.,

15. Gergely, P., and Lutz, L. A., "Maximum Crack Width in Reinforced Concrete Flexural Members," Causes, Mechanism, and Control of Cracking in Concrete, SP-20, American Concrete Institute, Detroit, 1968, pp. 1-17.

16. Hognestad, E., "High Strength Bars as Concrete Reinforcement, Part 2: Control of Cracking," Journal of PCA Research and Development Laboratories, Vol. 4, No. 1, January 1962, pp. 46-62.

17. Husain, S. I., and Ferguson, P. M., "Flexural Crack Width at the Bars in Reinforced Concrete Beams," Research Report No. 102-1F, Center for Highway Research, The University of Texas at Austin, June 1968.

18. Hognestad, E., "A Study of Combined Bending and Axial Load in Reinforced Concrete Members," Bulletin No. 399, University of Illinois Engineering Experiment Station, Urbana, November 1951.

19. Hognestad, E., Hanson, N. W., and McHenry, D., "Concrete Stress Distribution in Ultimate Strength Design," Journal of the American Concrete Institute, Proc. V. 52, December 1955, pp. 455-479.

20. Mattock, A. H., Kriz, L. B., and Hognestad, E., "Rectangular Concrete Stress Distribution in Ultimate Strength Design," Journal of the American Concrete Institute, Proc. V. 57, No. 8, February 1961, pp. 875-928.

21. Ramaley, D., and McHenry, D., "Stress-Strain Curves for Concrete Strained Beyond Ultimate Load," Laboratory Report No. SP-12, U. S. Bureau of Reclamation, Denver, 1947.

22. Whitney, C. S., "Plastic Theory of Reinforced Concrete Design," Journal of the Structural Division, ASCE, Trans. V. 107, 1942, pp. 251-326.

23. Kaar, P. H., "High Strength Bars as Concrete Reinforcement: Part 8: Similitude in Flexural Cracking of T-Beam Flanges," Journal of the PCA Research and Development Laboratories, Vol. 8, No. 2, May 1966, pp. 2-12.